R. & M. No. 3703

R. & M. No. 3703

MINISTRY OF DEFENCE (PROCUREMENT EXECUTIVE)

AERONAUTICAL RESEARCH COUNCIL
REPORTS AND MEMORANDA

Analysis of Mixed-Flow Rotor Cascades

By R. I. LEWIS, E. H. FISHER and A. SAVIOLAKIS
Dept. of Mechanical Engineering, University of Newcastle-upon-Tyne

LONDON: HER MAJESTY'S STATIONERY OFFICE
1972
PRICE £1·25 NET

Analysis of Mixed-Flow Rotor Cascades

By R. I. Lewis, E. H. Fisher and A. Saviolakis

Dept. of Mechanical Engineering, University of Newcastle-upon-Tyne

Reports and Memoranda No. 3703*
November, 1971

Summary.

Mixed-flow rotor cascades present a formidable design problem since rotational effects such as coriolis forces exclude the use of stationary cascade experimental data. This report discusses the general influence of these effects upon the energy transfer process and the parameters which govern the efficiency of a mixed-flow fan. An outline is presented of two cascade theories for predicting aerodynamic rotor cascade characteristics in detail. One deals with a restricted family of Joukowski type aerofoils providing a broad range of exact solutions by conformal transformation. The second theory involves the extension of Martensen's method to include relative eddy effects and also to allow for changes in meridional streamline thickness (AVR). This method which is applicable to any profile on any stream-surface of revolution is shown to produce accurate predictions compared with the exact solutions.

LIST OF CONTENTS

* Replaces A.R.C. 33 333.

1. Introduction.

The conventional design/analysis approach to axial turbomachines still leans heavily upon the quasi-two-dimensional model of superimposed cascade and meridional flows. Happily the straight cascade theoretical potential flow model then suits rotor and stator equally well since the governing equations for the relative flow are identical. Experimental straight cascade tests also have proved their worth as aids to design and performance prediction.

On the other hand mixed and radial flow machines pose completely different problems, as shown by the Euler pump equation for the fan illustrated in Fig. 1; expressed in terms of velocities measured relative to the rotor,

$$\begin{aligned}\Delta gH &= \Omega\,(r_2 V_{\theta 2} - r_1 V_{\theta 1}) \\ &= \Omega\,(r_2 V_{r_{\theta 2}} - r_1 V_{r_{\theta 1}}) + \Omega^2 (r_2^2 - r_1^2) \\ &= V_{B2}\left\{V_{r_{\theta 2}} - \left(\frac{r_1}{r_2}\right) V_{r_{\theta 1}}\right\} + V_{B2}^2\left\{1 - \left(\frac{r_1}{r_2}\right)^2\right\} \qquad (1) \\ &= \text{Work done due to fluid deflection} + \text{Work done due to coriolis forces}\end{aligned}$$

Head rise is dependent upon blade speed, V_{B2}, and change in peripheral whirl $V_{r_{\theta 1}}$ to $V_{r_{\theta 2}}$ as for axial machines. In addition ΔgH is dependent upon radial streamline shift (r_1/r_2). In the form presented above, part of the work done is entirely related to V_{B2} and (r_1/r_2) without any dependency upon blade profile shape. This contribution can be shown to precisely equal the work done by coriolis forces.

Stationary cascade models, both theoretical and experimental, are thus completely ruled out. Cascade potential flow analyses and boundary layer theories must be amended to include the effects of coriolis forces which can have a first order effect in both cases. Similar considerations must likewise be applied to prediction of turbulence propogation. Active research relevant to viscous effects and turbulence propogation is being undertaken by Johnston et alia[1] at Stanford University, Fowler at N.R.C.C.[2] and Professor Gruber and colleagues[3] at the Technical University of Budapest.

The present report sketches the outlines of two frictionless cascade analyses completed by the present authors. A conformal transformation method which provides exact solutions for a range of Joukowski conical cascades is summarised in Section 3.1. This analysis is reported in detail in Refs. 4 and 5. A completely general numerical method based upon extensions to Martensen's theory has also been developed and programmed for the calculation of arbitrary rotating compressor or turbine cascades, on an arbitrary surface of revolution with arbitrary meridional streamline thickness (AVR). A full report of this theory is in preparation but a brief outline is given in Section 3.2.

Before proceeding with these analyses some further remarks will be made in relation to performance assessment.

2. Assessment of Mixed Flow Fan Rotor Performance.

It is of interest to note that the total to total efficiency of a fan rotor can be expressed generally as

$$\eta_{TT} = f\left(\phi, \psi, \frac{r_1}{r_2}, \frac{A_2}{A_1}, \zeta_\infty\right), \qquad (2)$$

which after some analytical reduction from velocity triangle relationships becomes

$$\eta_{TT} = 1 - \zeta_\infty f_R, \qquad (3)$$

where ζ_∞ is the cascade loss coefficient based upon the vector mean relative velocity W_∞ as defined in

Fig. 1. The 'weighting coefficient', f_R, has the following convenient analytic form

$$f_R=\frac{1}{8\psi}\left\{\left(1+\frac{A_2}{A_1}\right)^2\phi^2+\left(1-\psi+\frac{r_1}{r_2}\right)^2\right\}, \tag{4}$$

which reduces to the more familiar form for axial fans ($r_1=r_2$) with constant annulus area ($A_2=A_1$),

$$f_{R\text{axial}}=\frac{1}{2\psi}\left\{\phi^2+\left(1-\frac{\psi}{2}\right)^2\right\}. \tag{4a}$$

In moving from axial machines to mixed-flow or centrifugal ones the additional design variables (r_1/r_2) and (A_2/A_1) are introduced, both of which influence the total to total rotor efficiency and therefore represent two more degrees of freedom available to the designer. For example, a first inspection of equation (4) suggests two new routes towards a low weighting coefficient and thus a high rotor efficiency, namely an increase in radial streamline shift r_2/r_1 and a reduction in annulus area A_2/A_1. Both avenues may be followed to some extent although increased r_2/r_1 involves a decrease in eye area if r_2 is held constant; likewise acceleration of the meridional flow to achieve reduced A_2/A_1 may present more difficult diffusion problems in the downstream stator.

Furthermore one must bear in mind that the losses ζ_∞ and also the form and stability of the (ϕ,ψ) characteristic will be influenced by adjustments to (r_2/r_1) and (A_2/A_1). Thus the frictional behaviour will be modified by coriolis forces introduced by the meridional streamline shift, (r_2/r_1), as well as by the general meridional velocity level which is controlled by (A_2/A_1). Indeed the essence of good design should surely be to play upon these available variables to obtain the 'optimum' design conditions.

The problems of design then fall into two categories which represent the chronological sequence of design:

(i) Selection of general machine duty coefficients (ϕ,ψ) and rough annulus shape (r_1/r_2) and (A_2/A_1).

(ii) Selection of detailed blade profile and annulus shapes to match the design duty (ϕ,ψ) with say high efficiency and stable performance.

Under (ii) the design problem breaks down as usual into potential flow analysis, boundary layer and loss prediction. Regrettably however the present state of knowledge of boundary layer growth and turbulence propagation in mixed-flow cascades leaves the field still wide open for exploration. Since, as we have seen, stationary cascade tests are ruled out for both (i) and (ii) the only alternatives are rotating cascade rigs or theoretical calculations. To this end the following research strategy is being carried out at Newcastle-upon-Tyne University, Department of Mechanical Engineering.

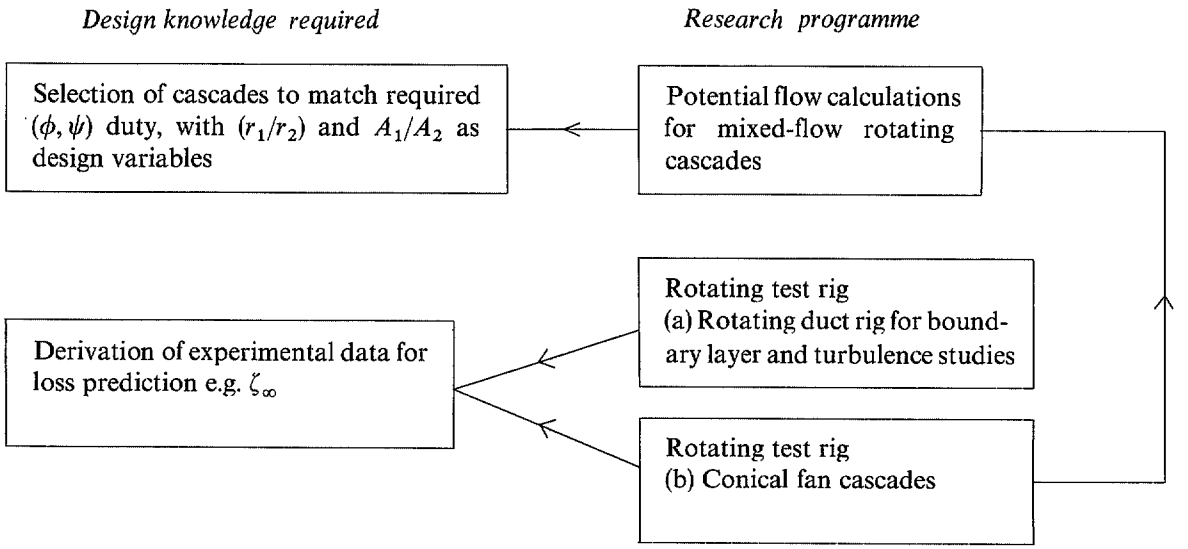

3. Treatment of Rotating Cascade Potential Flows.

The basic requirement following the conclusions of the previous section is for a blade to blade analysis for flow on an assumed surface of revolution defined by the meridional flow with continuous change in meridional streamline thickness within the blade region from leading edge to trailing edge. This can be achieved in one of two ways;

(a) by considering the irrotational absolute flow of the rotating blade system viewed by a stationary observer,

(b) by considering the rotational relative flow as viewed by an observer who rotates with the rotor.

The series of exact potential flow solutions derived by conformal transformations are based on (a). These are referred to in the next section. The general extended Martensen theory on the other hand is based upon consideration of (b) the relative flow. This will be explained in more detail in Section 3.2.

3.1 Exact Solutions for Joukowski Conical Cascades.

The off-set unit circle in the ζ-plane, Fig. 2 can be transformed into a Joukowski aerofoil in the z-plane by

$$z = d + c(\zeta + 1/\zeta), \tag{5}$$

and from there into a conical cascade on the z-surface with N blades and semicone angle Ψ by

$$z = Z^{N \operatorname{cosec} \Psi}. \tag{6}$$

The threefold geometrical limitation here is first of available profile, and second of zero stagger and third of constant meridional streamline thickness. Nevertheless an infinite range of cambers, profile thickness and pitch/chord ratios is still possible. Typical samples of symmetrical and cambered profiles are shown in Figs. 3 and 4 which illustrate the effects of the two eccentricities of the unit circles ε_1 and ε_2 responsible primarily for thickness and camber respectively. A typical centrifugal rotor is shown in Fig. 5 for $\Psi = 90°$, $r_1/r_2 = 0{\cdot}6$, $\varepsilon_1 = 0{\cdot}02$ and $\varepsilon_2 = 0{\cdot}5$.

3.2 Extended Martensen Method for Arbitrary Mixed-Flow Rotating Cascades.

To provide a completely generalised method for curved meridional flows with variable meridional streamline thickness, it was considered more simple to transform the conical cascade in the Z-plane into an infinite straight cascade in the $\bar{\zeta}$-plane by means of the well known transformation

$$\begin{aligned} d\bar{\eta} &= d\Theta, \\ d\bar{\xi} &= \frac{ds}{r} = \frac{dr}{r \sin \Psi} \end{aligned} \tag{7}$$

where (x, r, Θ) are cylindrical coordinates and s is distance measured along the meridional streamlines. The absolute velocity transformation follows directly

$$u_{\bar{\zeta}} - iv_{\bar{\zeta}} = r(u_Z - iv_Z). \tag{8}$$

Although conformal transformations are normally applied to irrotational solenoidal flows, it is possible to prove that flow fields containing source and vortex singularities may also be conformally transformed provided the singularities are transformed point by point with no change in strength. If the field is rotational however, the vorticity (i.e. distributed vortex strength per unit area) is changed in

strength on transformation. Thus for the relative eddy of a mixed-flow rotor, Fig. 1

$$\gamma_{\bar{\xi}} = r^2 \gamma_Z$$

$$= -r^2 \, 2\Omega \sin \Psi \,. \tag{9}$$

The $\bar{\zeta}$-plane thus contains a vorticity distribution given by equation (9) upstream, downstream and in the gap between the blades, Fig. 6. By the principle of superposition, this flow can be replaced by vorticity distributed throughout the whole of the cascade region which is constant in the pitchwise direction, minus a vorticity in the interior blade region. These two vorticities introduce disturbance velocities $q_{\Omega\infty}(\bar{\xi})$ and $q_{\Omega i}(\bar{\xi}, \bar{\eta})$ respectively.

The change in meridional streamline thickness may be approximated by a source distribution in the flow field outside the blades of constant strength in a pitchwise direction. This effect is illustrated in Fig. 7 where the varying throughflow velocity $u(\bar{\xi})$ in a convergent duct is equivalent for all $\bar{\xi}$ to the flow in a parallel duct with mean velocity U_∞ and a disturbance velocity $u_{\sigma_\infty}(\bar{\xi})$ induced by source distributions. The sources may be removed from the blade profiles by superposing an equivalent distribution of sinks in these regions and, if the resultant disturbance velocity is $q_{\sigma i}(\bar{\xi}, \bar{\eta})$, the total velocity induced by the free stream and the source and vorticity distributions is

$$q = (U_\infty + u_{\sigma_\infty} + u_{\Omega i} + u_{\sigma i}) +$$

$$+ i\,(V_\infty + v_{\Omega_\infty} + v_{\Omega i} + v_{\sigma i}) \,. \tag{10}$$

Special techniques have been developed for computing the vorticity and source velocities $(u_{\Omega i}, v_{\Omega i})$ and $(u_{\sigma i}, v_{\sigma i})$. The cascade is divided into a number of strips, Fig. 8, and each segment of blade is represented by a trapezium of uniform source strength and vorticity. Developments from Ackeret's[6] Fourier series have led to solutions for the consequent induced velocities.

Martensen's method is based upon a Fredholm integral equation which states that the fluid velocity inside the aerofoil (replaced by a peripheral vorticity distribution $\gamma(S)$) is zero. Thus for location S_m on the aerofoil, Fig. 9

$$-\frac{\gamma(S_m)}{2} + \frac{1}{2\pi} \oint \gamma(S_n) \, K(S_m, S_n) \, dS_n = -\left\{ U_\infty \left(\frac{dx}{dS}\right)_m + V_\infty \left(\frac{dy}{dS}\right)_m \right\}, \tag{11}$$

where $K(S_m, S_n)$ is a coupling coefficient which links S_m and S_n and for a cascade is given by

$$K(S_m, S_n) = \frac{\pi}{t} \left\{ \frac{y'_m \sinh \frac{2\pi}{t}(x_m - x_n) - x'_m \sin \frac{2\pi}{t}(y_m - y_n)}{\cosh \frac{2\pi}{t}(x_m - x_n) - \cos \frac{2\pi}{t}(y_m - y_n)} \right\}$$

where

$$y'_m = \left(\frac{dy}{dS}\right)_m \text{ and } x'_m = \left(\frac{dx}{dS}\right)_m . \tag{12}$$

The r.h.s. of (11) represents the displacement flow, i.e. uniform stream W_∞ into which the cascade is immersed.

For the cascade under consideration with the additional Ω and σ disturbances, the r.h.s. of the equation is simply modified to

$$\text{r.h.s.} = -\left\{ (U_\infty + u_{\sigma_\infty} + u_{\Omega i} + u_{\sigma i}) \left(\frac{dx}{dS}\right)_m + (V_\infty + v_{\Omega_\infty} + v_{\Omega i} + v_{\sigma i}) \left(\frac{dy}{dS}\right)_m \right\}, \tag{13}$$

where $u_{\sigma\infty}$ is a function of streamsheet thickness and blade blockage and $v_{\Omega\infty}$ follows directly from equation (9)

$$\gamma_{\bar{\zeta}} = -2\,\Omega r^2 \sin\bar{\psi}$$

$$= \frac{d\,v_{\Omega_\infty}}{d\bar{\zeta}}$$

$$= \frac{d\,v_{\Omega_\infty}}{dr} \,.\, r \sin\bar{\psi} \text{ from equation (7).}$$

Thus

$$v_{\Omega_\infty} = -\Omega r^2 + \text{constant}\,. \tag{14}$$

The constant may be evaluated by considering the velocity at the leading edge. If the whirl velocity at inlet to the continuous vortex distribution, or 'displacement flow' of Fig. 6, is V_{θ_1} then

$$v_{\Omega_{\infty 1}} = -\Omega r_1^2 + \text{const}$$

$$= V_{\theta_1}\,.$$

Thus elsewhere within the blade row

$$v_{\Omega_\infty} = -\Omega(r^2 - r_1^2) + V_{\theta_1} \tag{15}$$

Thus once again the parameter $\Omega(r^2 - r_1^2)$, shown in equation (1) to be associated entirely with coriolis forces, enters into our analysis as an additional disturbance due to the relative eddy $2\Omega \sin \Psi$, Fig. 1. It is extremely interesting to note this direct equivalence of coriolis forces in the rotating system to the relative eddy introduced into our stationary theoretical cascade model.

Sufficient analysis has been provided here to explain the central principles. Solution of the Fredholm integral equation proceeds along similar lines to the conventional Martensen analysis. The remainder of this report is concerned with the presentation of a number of cases which have been computed.

4. Comparison of Results.

Results obtained from the numerical and transformation analyses are compared in Figs. 10 to 14.

Slip factors for a range of centrifugal rotors are shown in Fig. 10. Blade profiles were calculated by the conformal transformation method for fixed values of circle eccentricity, ε_1 and ε_2, and consequently each point on the curves represents a different symmetrical profile. The range of aerofoils obtained for 8-bladed rotors is shown in Fig. 3 and blade co-ordinates are given in Table 1. Blade thickness varies from approximately 18 to 30 per cent of chord but in all cases the slip factors predicted by the two methods agree well. Equally striking is the agreement between surface velocity distributions shown in Fig. 11. In this case, a conical rotor with eight symmetrical blades, semi-cone angle equal to 60 degrees, and radius ratio 0·6 was subjected to 20 degree prewhirl.

Similar results have been obtained for cambered blades. Solutions have been computed for the eight bladed centrifugal rotor shown in Fig. 5 with the selection of cambered blades illustrated in Fig. 4. Corresponding blade co-ordinates are listed in Table 2. Velocity distributions and outlet angles are given in Figs. 12 to 14 and in all cases close agreement is obtained between the numerical and conformal transformation solutions.

Results obtained from the numerical program for rotors of arbitrary geometry operating at design point have been compared with those from a National Engineering Laboratory program, based on the work of Railly[7]. Velocity distributions obtained for two blade designs on the arbitrary streamsurface shown in Fig. 15 are plotted in Figs. 16 and 17. The distribution in Fig. 16 is for a constant streamsheet

thickness whereas that in Fig. 17 is computed for a thickness ratio of 1:0·84. A similar comparison for an eight-bladed centrifugal rotor of radius ratio 1:2, subjected to a more extreme streamsheet thickness reduction of 1:0·66, is shown in Fig. 18. In all cases the two methods agree well, but the numerical program gives much better definition around the blade leading edge.

Evidence of the validity of the numerical program for thin blade profiles is presented in Figs. 19 and 20. Fig. 19 shows two blade sections of different thickness which have been used to compute approximations to the Weinig cascade 'lattice coefficient' for flat plate cascades. These values are plotted in Fig. 20 against the exact values given by Wislicenus[8]. For the two stagger angles considered, $\lambda = 30$ and 60 degrees, it is evident that as the blade thickness tends to zero fair agreement is obtained.

The final set of numerical results is presented in Fig. 21. Velocity distributions and outlet angles are given for a seven bladed centrifugal log-spiral machine of spiral angle 50 degrees and radius ratio 1:2. The three distributions shown correspond to constant streamsheet thickness, a decrease in thickness of 1:0·83, and an increase of 1:1·25. Although these results are not directly comparable with any other known solution, the general trend is consistent with the findings of Pollard and Horlock[9], who reported a decrease in deviation when an accelerating flow was introduced into a stationary cascade. It would appear that this effect could be used to advantage when designing annuli for mixed-flow pumps and fans.

All the evidence presented suggests that the surface singularity numerical program developed at Newcastle University yields results which are consistent with other known solutions and it would appear that the program may now be used for practical design, bearing in mind that it provides only a frictionless potential flow solution to the problem of blade to blade flow.

LIST OF SYMBOLS

A	Annulus area
c, d	Coefficients in transformation equation (5)
C_{L_0}	Lift coefficient of isolated aerofoil
C_L	Lift coefficient of aerofoil in cascade
f_R	Rotor loss weighting coefficient given by equation (4)
gH	Head rise
k	Annulus area ratio
$K(S_m, S_n)$	Cascade coupling coefficient
K_W	Weinig 'Lattice coefficient'
N	Number of rotor blades
q	Disturbance velocity
r, x, Θ	Cylindrical polar coordinates
$\bar{r}, \theta$	Polar co-ordinates in z-plane (Fig. 2.2)
$R, \Theta \sin \Psi$	Polar coordinates in Z-plane
S	Distance along blade profile measured A.C.W. from trailing edge
s	Meridional distance
t	Cascade pitch
u, v	Cartesian components of velocity
$\bar{u}, \bar{v}$	Polar components of velocity
U_∞, V_∞	Components of cascade vector mean velocity W_∞ in x, y directions
V, V_r	Absolute and relative velocities
V_B	Blade speed
V_S	Surface velocity and meridinal velocity
x, y	Coordinates in straight cascade plane
	Coordinates in single Joukowski aerofoil z-plane

x', y'	Derivatives of x and y w.r.t. S.
z	Single Joukowski aerofoil plane
Z	Conical cascade plane
α	Absolute flow angle
β	Relative flow angle
γ	Distributed vorticity due to relative eddy
$\gamma(S)$	Blade profile peripheral vorticity
Γ	Point vortex
ε	Eccentricity of the origin of coordinates, O, from the centre of the blade circle, M, (Fig. 2.3)
$\varepsilon_1, \varepsilon_2$	Components of eccentricity
ζ	Unit circle plane
$\bar{\zeta}$	Infinite straight cascade $(\bar{\xi}, \bar{\eta})$ plane
ζ_∞	Cascade loss coefficient $\Delta p_o / \frac{1}{2}\rho W_\infty^2$
η_{TT}	Total to total efficiency
λ	Stagger angle
λ_S, β_S	Polar co-ordinates in ζ-plane with origin at M (Fig. 2.3)
μ_S, α_S	Polar co-ordinates in ζ-plane with origin at 0 (Fig. 2.3)
$\bar{\xi}, \bar{\eta}$	Coordinates in ζ plane
ϕ	Flow coefficient
ψ	Head coefficient
$\bar{\psi}$	Semi-cone angle
Ω	Speed of rotation (radians/sec)

Suffixes

1, 2	Leading and trailing edge locations
∞	Disturbance velocities due to singularities in cascade region with blades removed

i	Disturbance velocities due to singularities within the blade profile
m, n	At locations S_m, S_n on blade profile
s	Along meridional surface
z	In z plane
Z	In Z plane
$\bar{\zeta}$	In $\bar{\zeta}$ plane
θ	In θ, whirl, direction
σ	Velocities due to source distributions
Ω	Velocities due to relative eddy vorticity

REFERENCES

No.	*Author(s)*	*Title, etc.*
1	J. P. Johnston	The effects of rotation on boundary layers in turbomachine rotors. Symposium on 'Fluid Mechanics and Design of Turbomachinery', Pennsylvania State University. September, 1970.
2	H. S. Fowler	Experiments on the flow processes in simple rotating channels. National Research Council of Canada. Mechanical Engineering Report ME–229, Ottawa. January, 1969.
3	J. Gruber and E. Litvai . .	An investigation of the effects caused by fluid friction in radial impellers. Proceedings of the Third Conference on Fluid Mechanics and Fluid Machinery. Budapest, 1969.
4	E. H. Fisher and R. I. Lewis . .	Exact solutions for conical mixed-flow rotors. Part I: Symmetrical profiled blades. N.E.L. Report No. 498. 1971.
5	E. H. Fisher and R. I. Lewis . .	Exact solutions for conical mixed-flow rotors. Part II: Cambered blades of finite thickness. Report No. Tb.18, University of Newcastle-upon-Tyne. Department of Mechanical Engineering. 1971. N.E.L. Report to be published.
6	J. Ackeret	Zum Entwurf Dicht Stehender Schaufelgitter Schweitz Bauztg. Vol. 120, No. 9. Ministry of Aviation Translation. RTP 2007. 1942.
7	J. W. Railly, J. M. Houlton and K. Murugesan . .	A solution to the direct problem of flow in an arbitrary mixed-flow turbomachine. N.E.L. Report No. 413. 1969.
8	G. F. Wislicenus	*Fluid mechanics of turbomachinery.* Vol. 1. Dover Publications Inc., 2nd Edition. 1965.
9	D. Pollard and J. H. Horlock	A theoretical investigation of the effect of change in axial velocity on the potential flow through a cascade of aerofoils. A.R.C. CP No. 619. 1962.

TABLE I

Blade Profile Co-ordinates.

Co-ordinates with $N=8$, $\varepsilon=0{\cdot}1$.

% chord from l.e.	Blade half-thickness (% chord) for $R_1/R_2=$ 0·2	0·4	0·6	0·8
0	0	0	0	0
1·25	2·83	4·40	4·72	2·99
2·5	3·84	6·42	6·58	4·13
5·0	5·05	8·84	8·82	5·60
7·5	5·99	10·40	10·26	6·55
10·0	6·69	11·59	11·21	7·34
15·0	7·80	13·51	12·16	8·03
20·0	8·84	14·16	12·35	8·39
25·0	9·76	14·27	12·08	8·44
30·0	10·57	13·95	11·52	8·28
35·0	11·15	13·17	10·79	7·94
40·0	11·39	12·09	9·93	7·47
45·0	11·13	10·85	9·01	6·93
50·0	10·35	9·57	8·05	6·31
55·0	9·19	8·31	7·12	5·62
60·0	7·88	7·10	6·14	4·91
65·0	6·57	5·95	5·20	4·17
70·0	5·34	4·87	4·25	3·44
75·0	4·20	3·84	3·34	2·71
80·0	3·14	2·87	2·48	2·00
85·0	2·15	1·95	1·68	1·34
90·0	1·25	1·05	0·95	0·75
92·5	0·84	0·75	0·62	0·49
95·0	0·48	0·42	0·35	0·26
97·5	0·17	0·15	0·11	0·10
98·75	0·06	0·05	0·05	0·03
100	0	0	0	0

Data in the tables have been interpolated graphically and are therefore of limited accuracy. Co-ordinates may be calculated to any required accuracy by reference to (4) and (5).

TABLE 2

Co-ordinates with $N=8$, $\varepsilon_1=0{\cdot}04$, $R_1/R_2=0{\cdot}6$.

	$\varepsilon_2=0{\cdot}1$		$\varepsilon_2=0{\cdot}3$		$\varepsilon_2=0{\cdot}5$	
% chord from l.e.	y (lower)	y (upper)	y (lower)	y (upper)	y (lower)	y (upper)
0	0	0	0	0	0	0
1·25	−2·16	3·04	−1·61	4·48	−1·25	6·81
2·50	−2·92	4·13	−2·09	5·91	−1·50	8·49
5·00	−3·67	5·51	−2·22	7·91	−0·96	10·96
7·50	−3·97	6·41	−1·86	9·33	0·12	12·80
10·0	−4·02	7·03	−1·29	10·43	1·40	14·26
15·0	−3·76	7·77	0·10	12·02	3·98	16·46
20·0	−3·25	8·11	1·53	13·06	6·31	18·02
25·0	−2·65	8·21	2·87	13·75	8·31	19·15
30·0	−2·02	8·15	4·07	14·19	10·00	19·96
35·0	−1·40	7·98	5·13	14·42	11·41	20·50
40·0	−0·82	7·74	6·03	14·48	12·56	20·82
45·0	−0·28	7·43	6·77	14·40	13·46	20·93
50·0	0·20	7·07	7·36	14·17	14·13	20·83
55·0	0·63	6·66	7·78	13·79	14·55	20·52
60·0	0·99	6·19	8·02	13·26	14·71	19·98
65·0	1·27	5·67	8·08	12·56	14·59	19·19
70·0	1·48	5·09	7·93	11·67	14·16	18·10
75·0	1·59	4·44	7·53	10·55	13·38	16·66
80·0	1·59	3·72	6·86	9·17	12·18	14·81
85·0	1·47	2·91	5·87	7·50	10·47	12·45
90·0	1·19	2·02	4·48	5·46	8·10	9·40
92·5	0·99	1·54	3·61	4·28	6·60	7·56
95·0	0·73	1·04	2·59	2·98	4·82	5·42
97·5	0·41	0·52	1·40	1·55	2·68	2·93
98·75	0·22	0·26	0·73	0·79	1·43	1·53
100·0	0·0	0·0	0·0	0	0	0

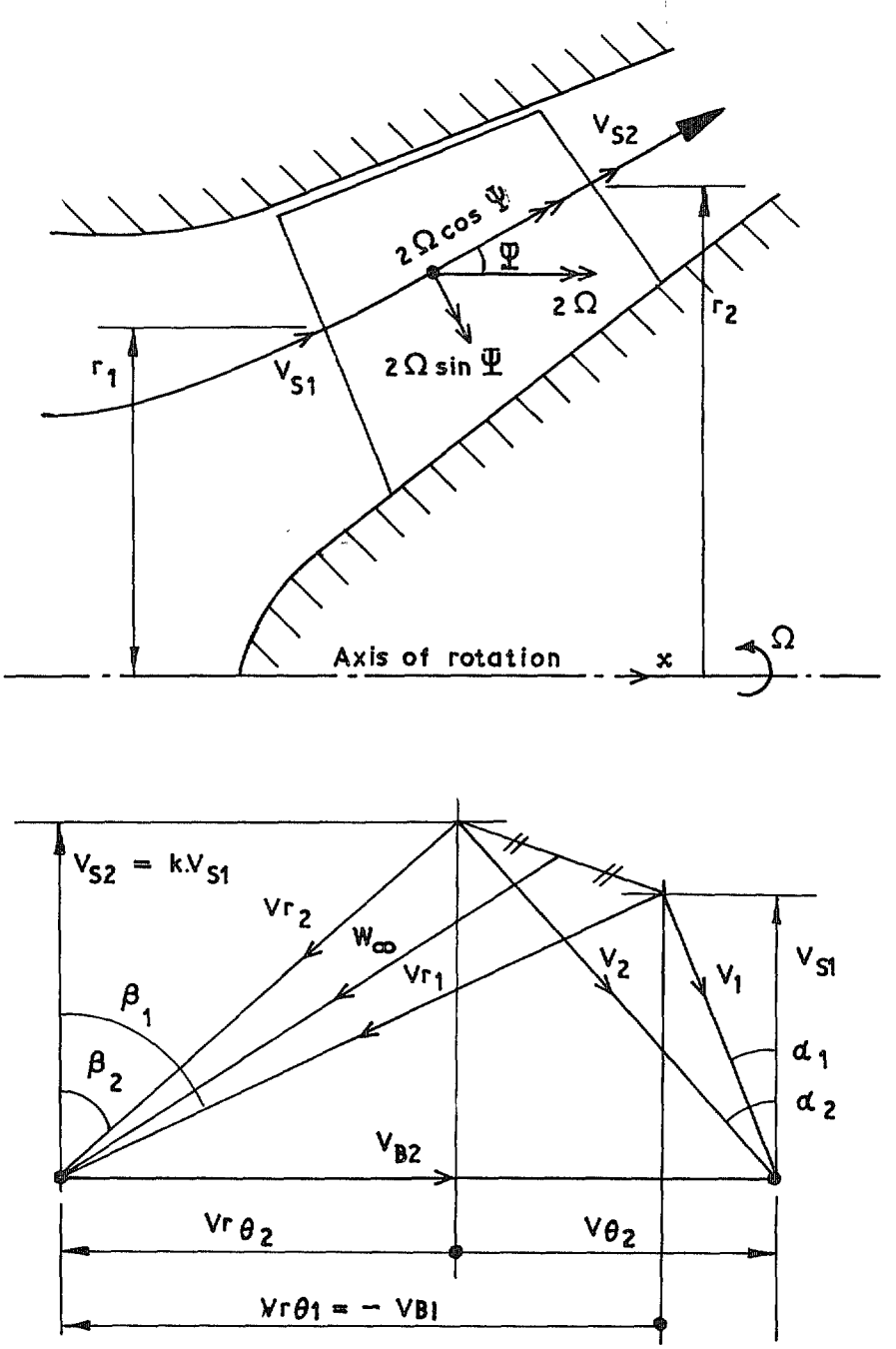

FIG. 1. Annulus configuration and velocity triangles for a mixed flow pump or fan rotor.

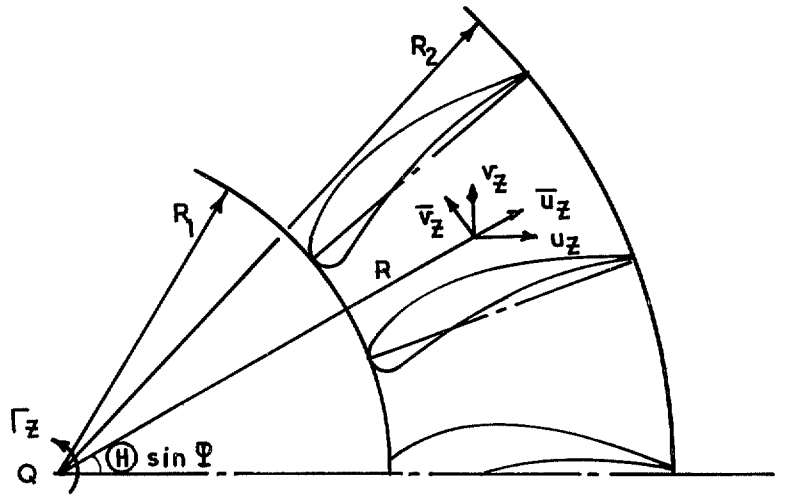

FIG. 2.1. $\mathcal{Z}$-plane, development of conical streamsurface.

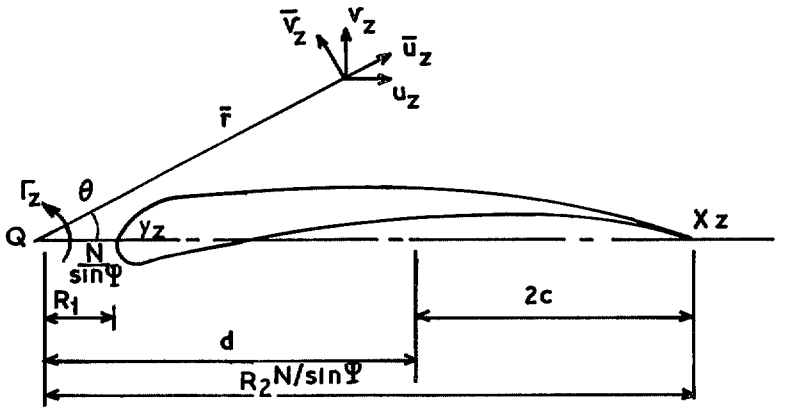

FIG. 2.2. z-plane or 'single blade' plane.

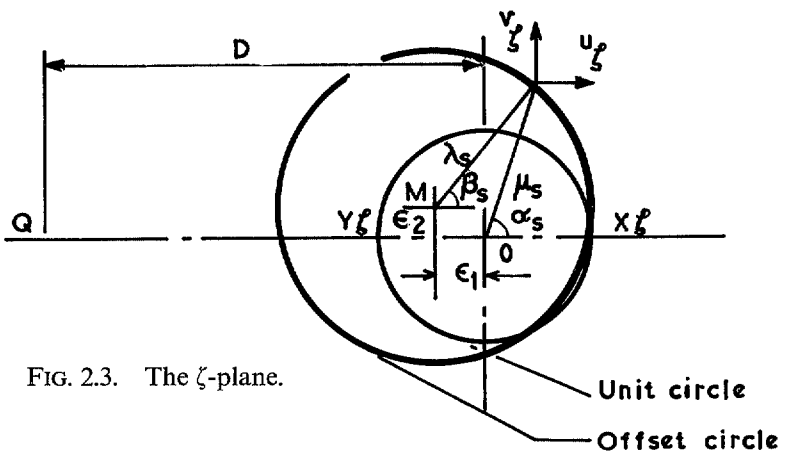

FIG. 2.3. The ζ-plane.

FIG. 2. The transformations.

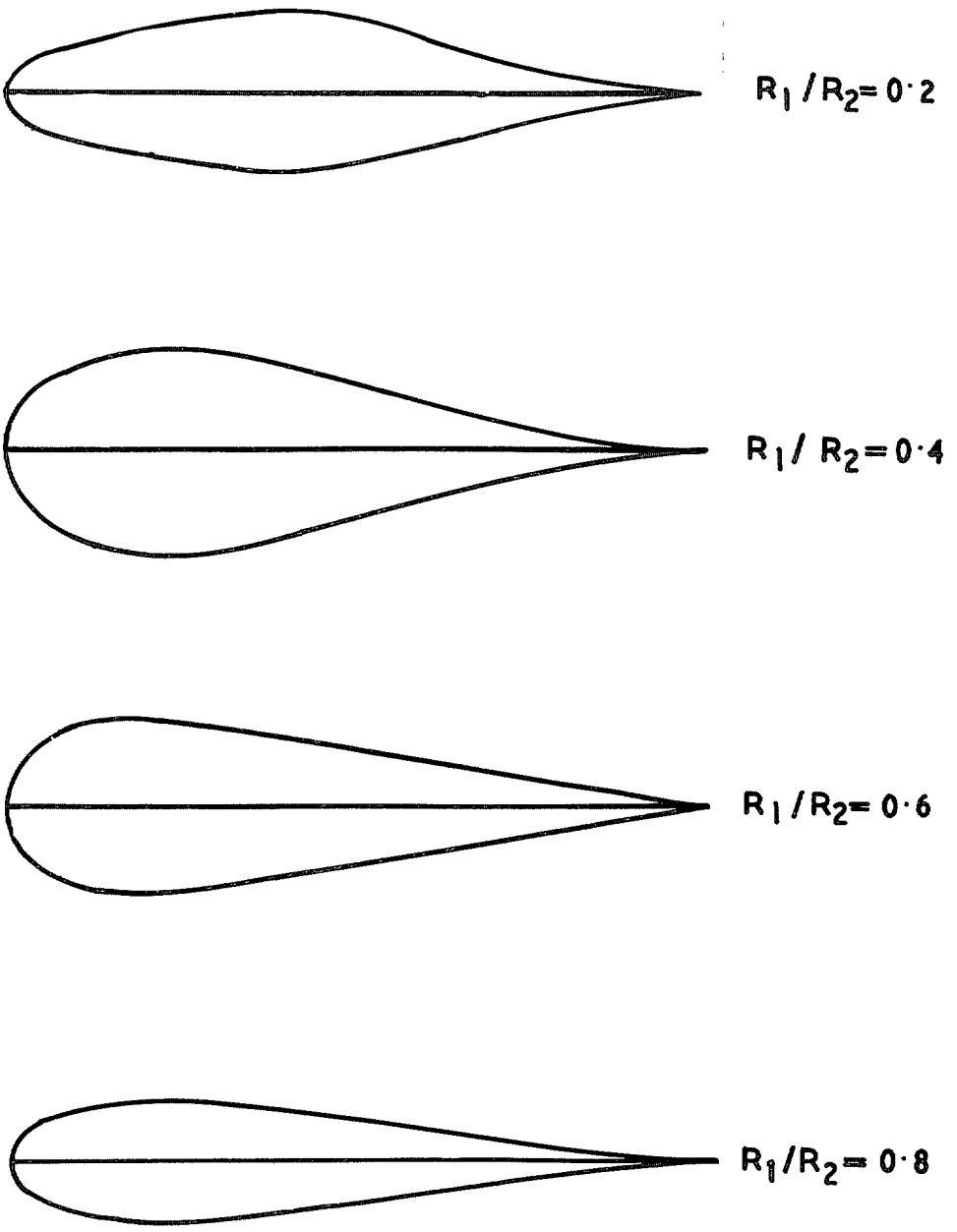

FIG. 3. Variation of blade profile with R_1/R_2, $\varepsilon = 0{\cdot}1$, $N = 8$.

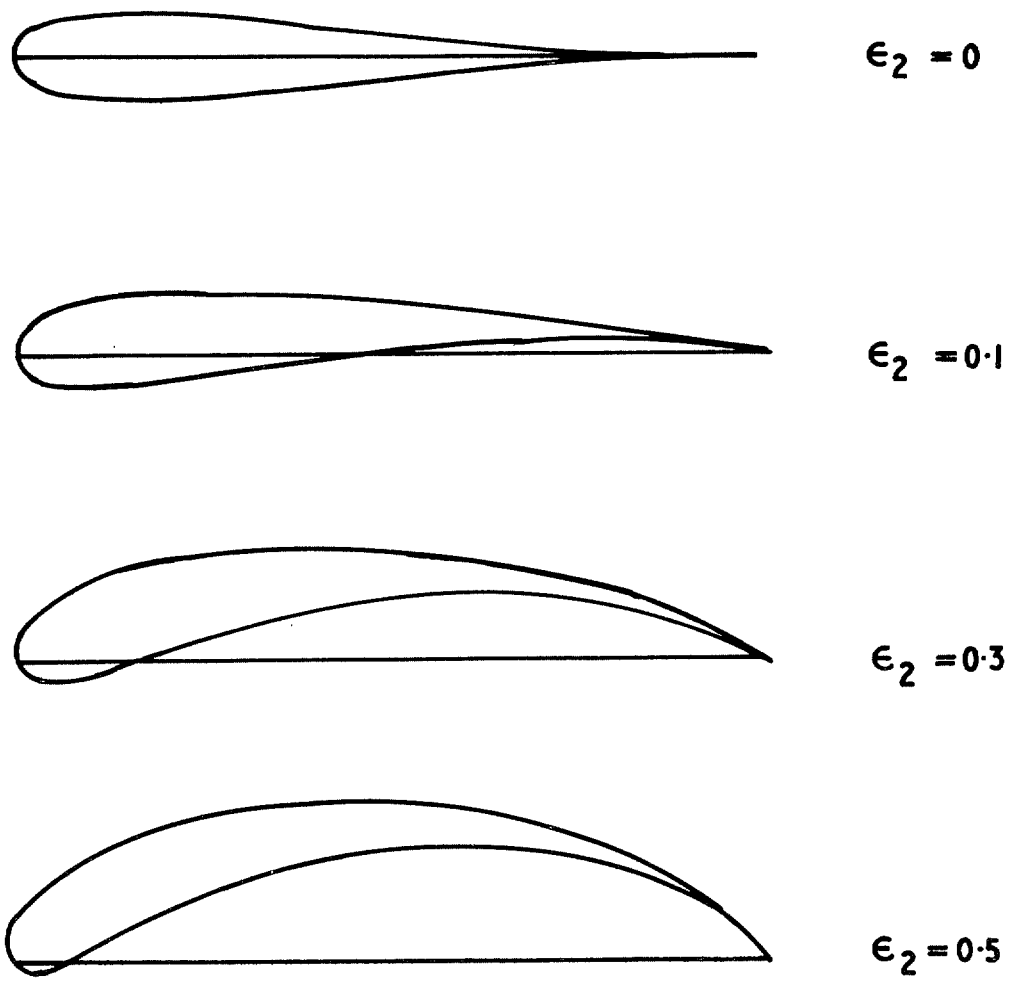

FIG. 4. The influence of ε_2 upon camber. $N = 8$, $\varepsilon_1 = 0{\cdot}04$, $R_1/R_2 = 0{\cdot}6$.

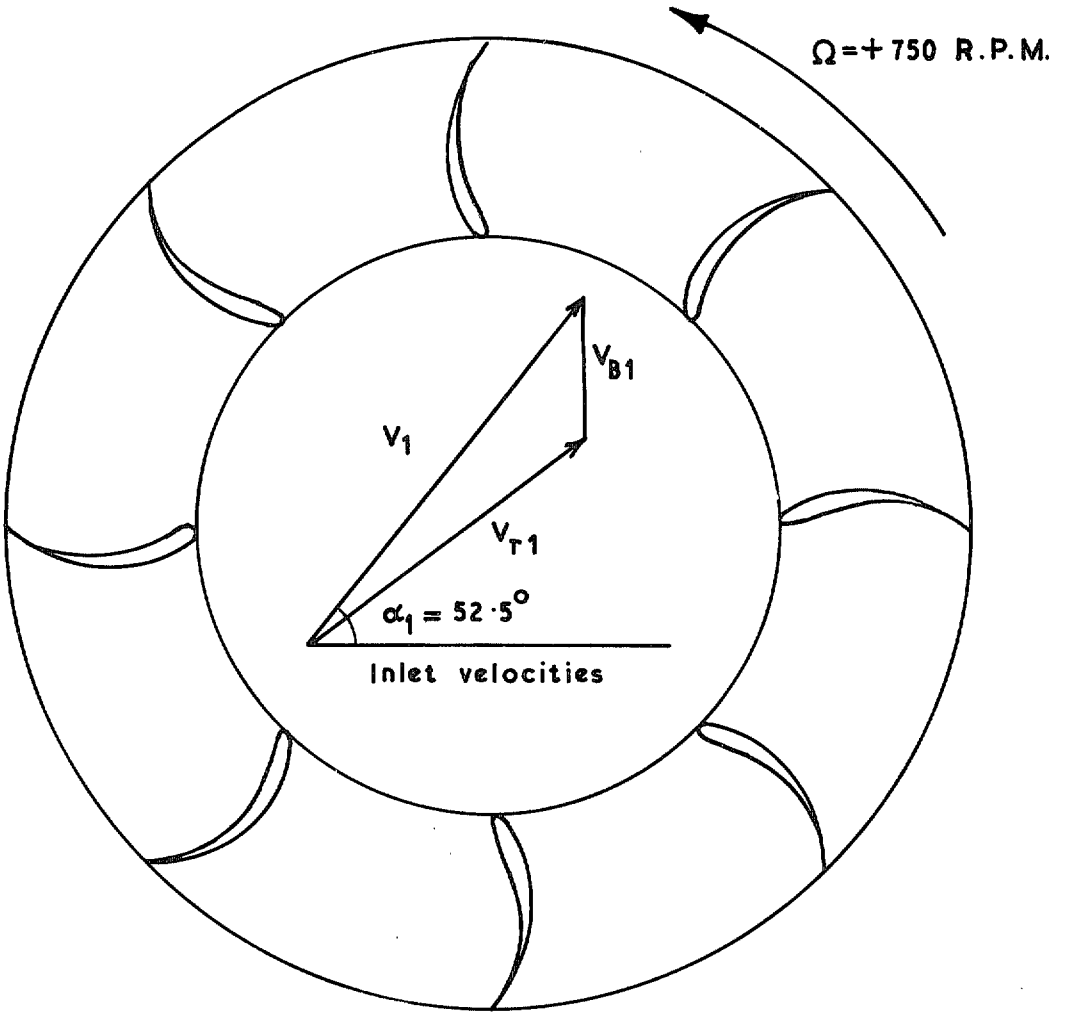

FIG. 5. Centrifugal rotor. $N=8$, $\varepsilon_1=0{\cdot}02$, $\varepsilon_2=0{\cdot}5$, $R_1/R_2=0{\cdot}6$, $\Psi=90°$.

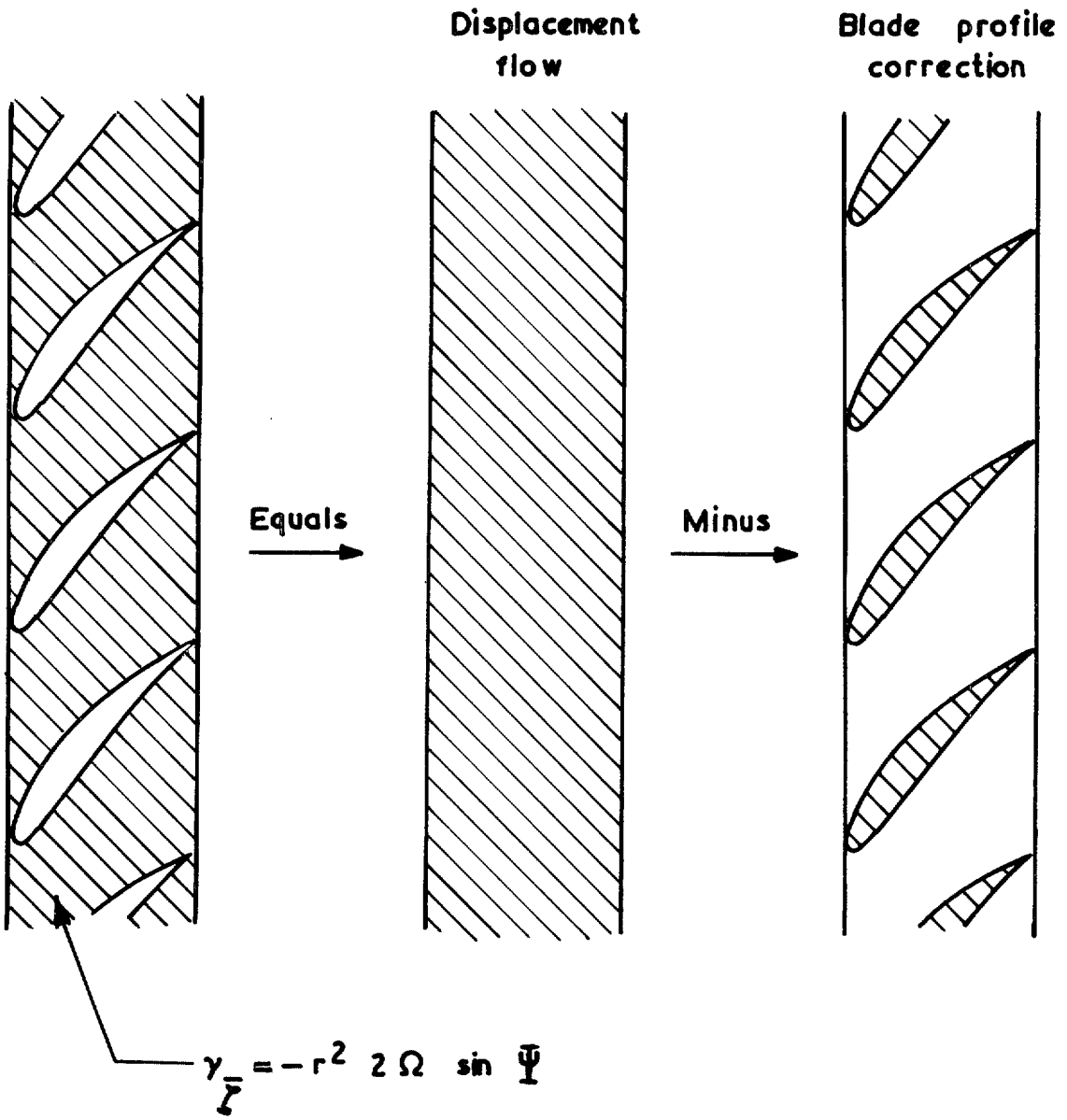

FIG. 6. Vorticity $\gamma_{\bar{\zeta}}$ in $\bar{\zeta}$ plane due to relative eddy represented by superposition of two flows.

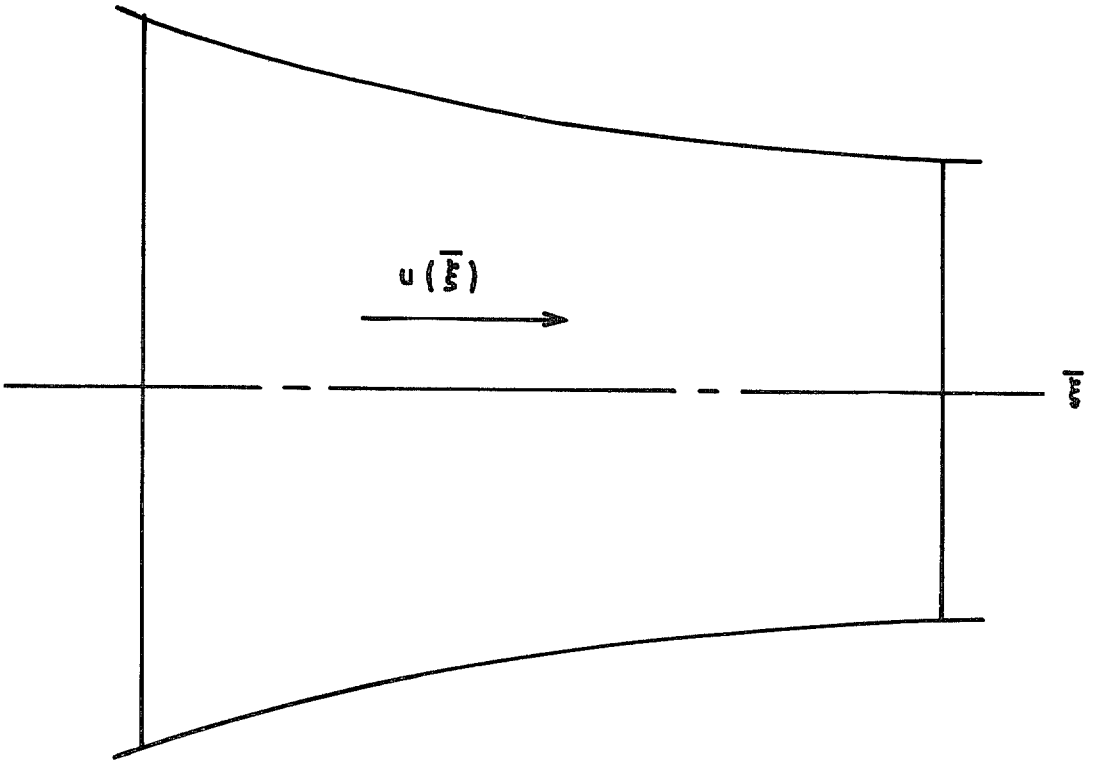

7·1 convergent duct

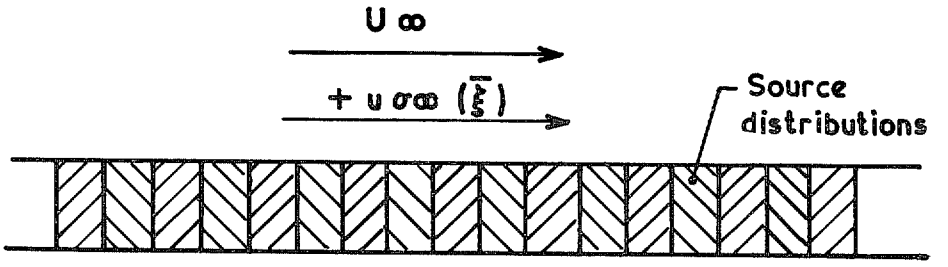

7·2 equivalent parallel duct with source distributions

FIG. 7. Representation of flow in a convergent duct by source distributions in a parallel duct.

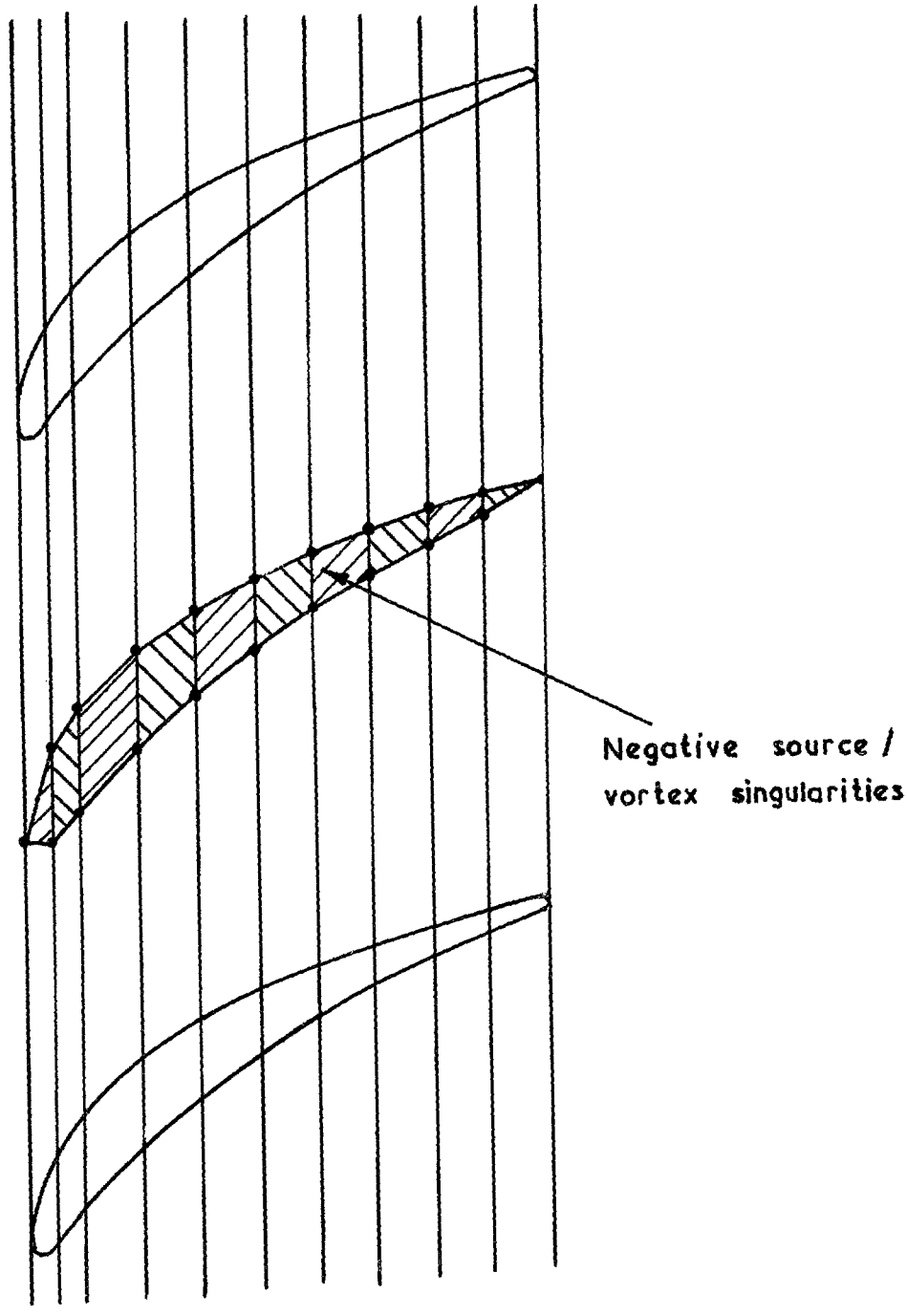

FIG. 8. Trapezium representation of blade profile for removal of internal source/vortex singularities.

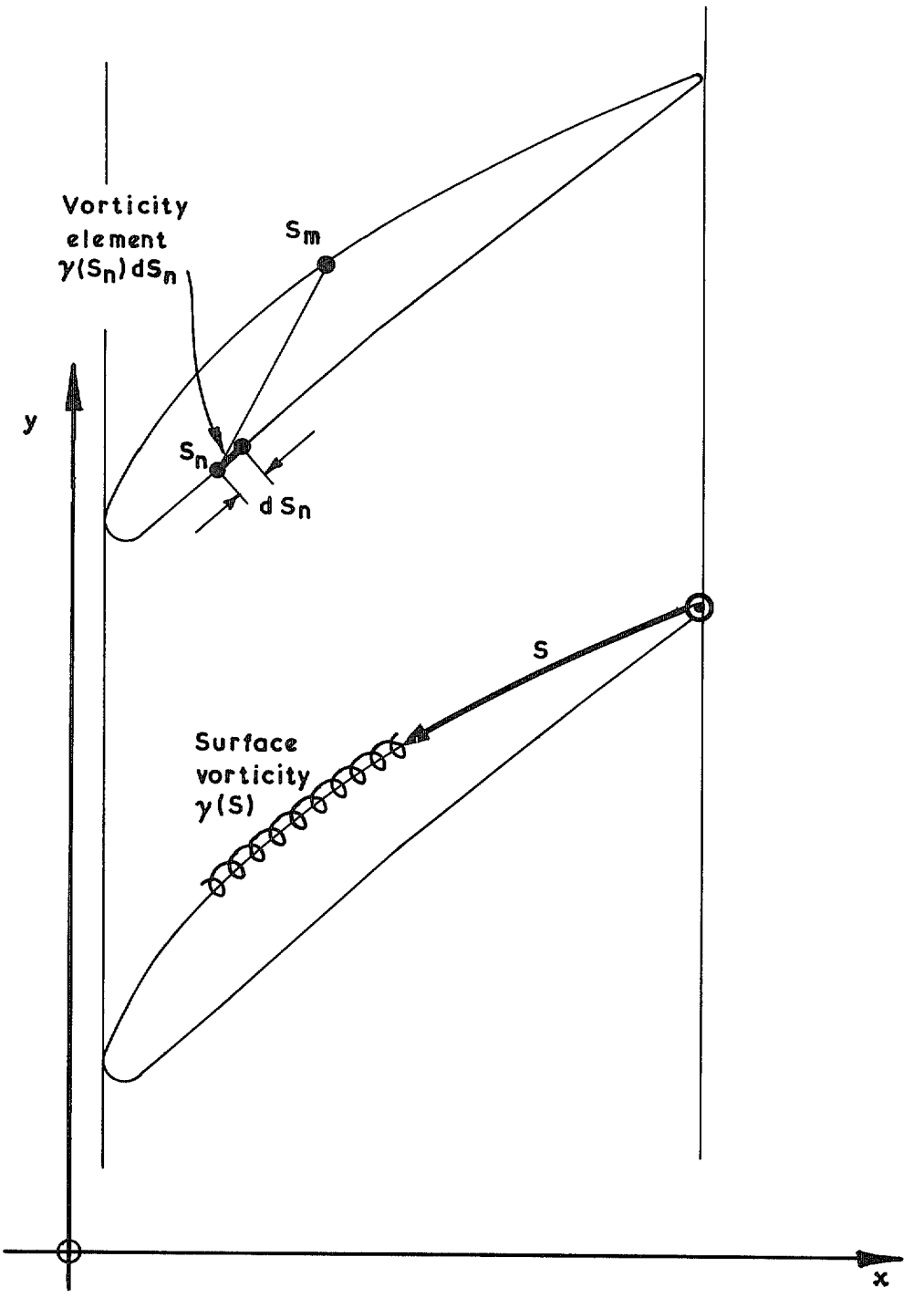

FIG. 9. Representation of cascade by distribution of surface vorticity.

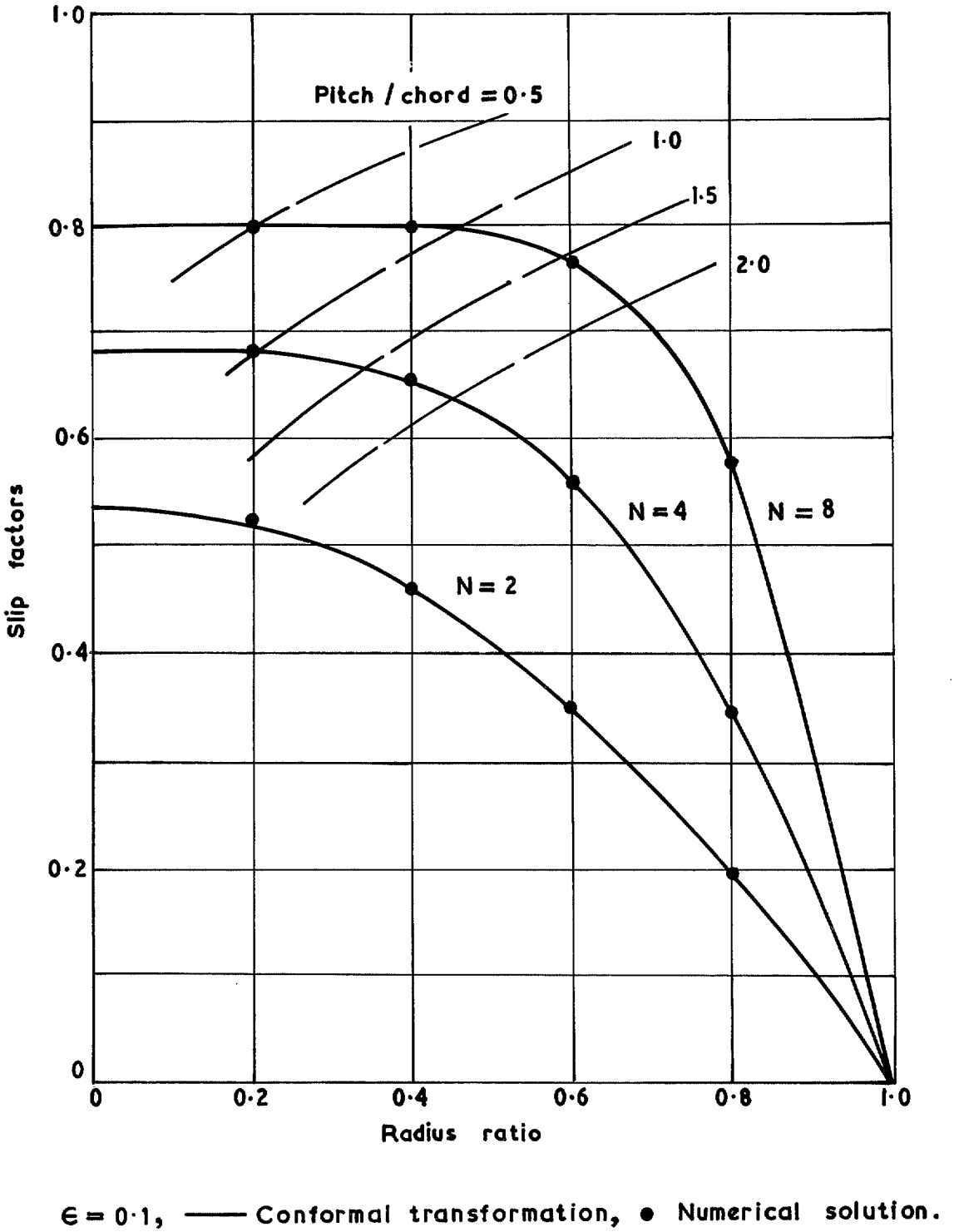

FIG. 10. Comparison of slip factors.

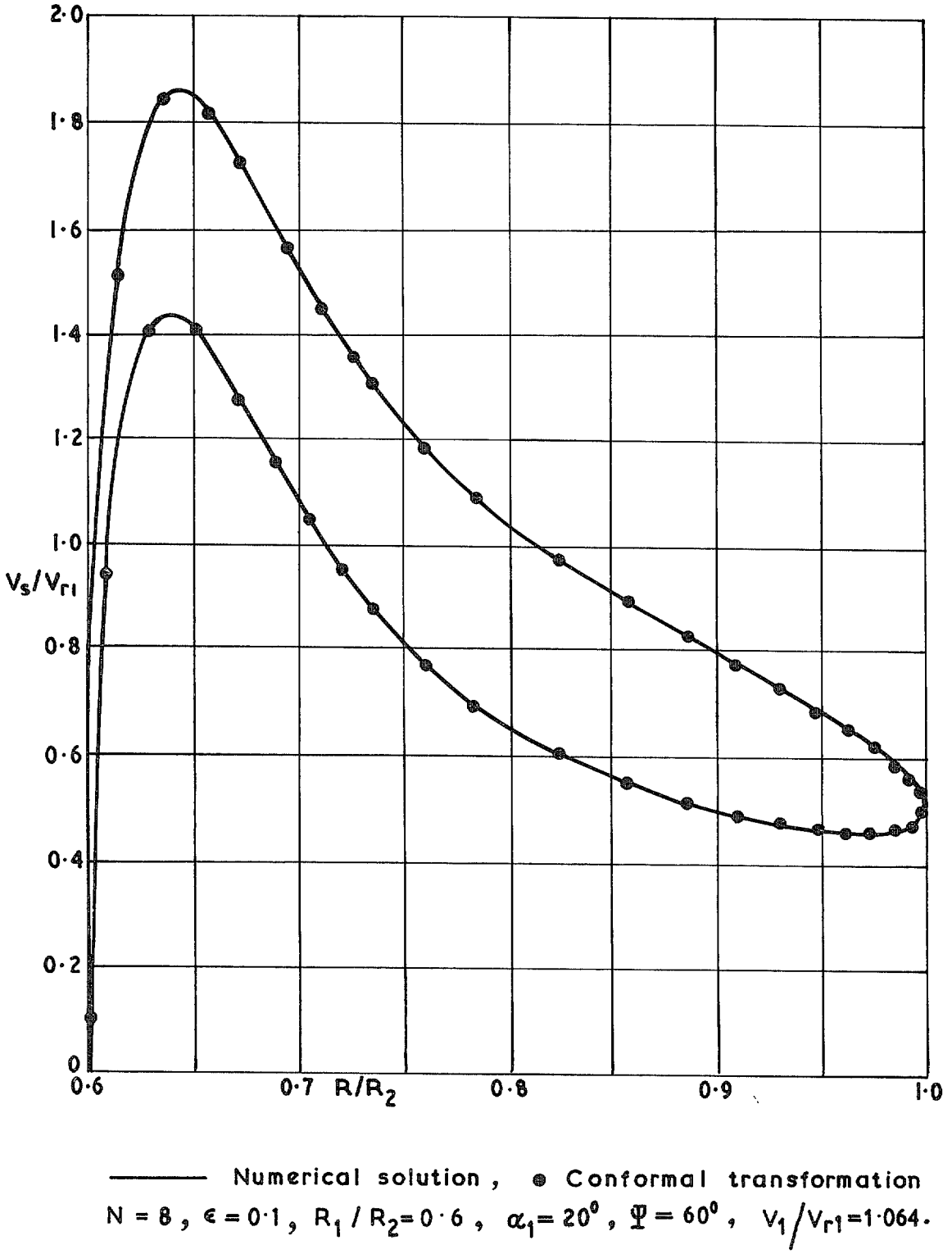

FIG. 11. Comparison of surface velocity distributions.

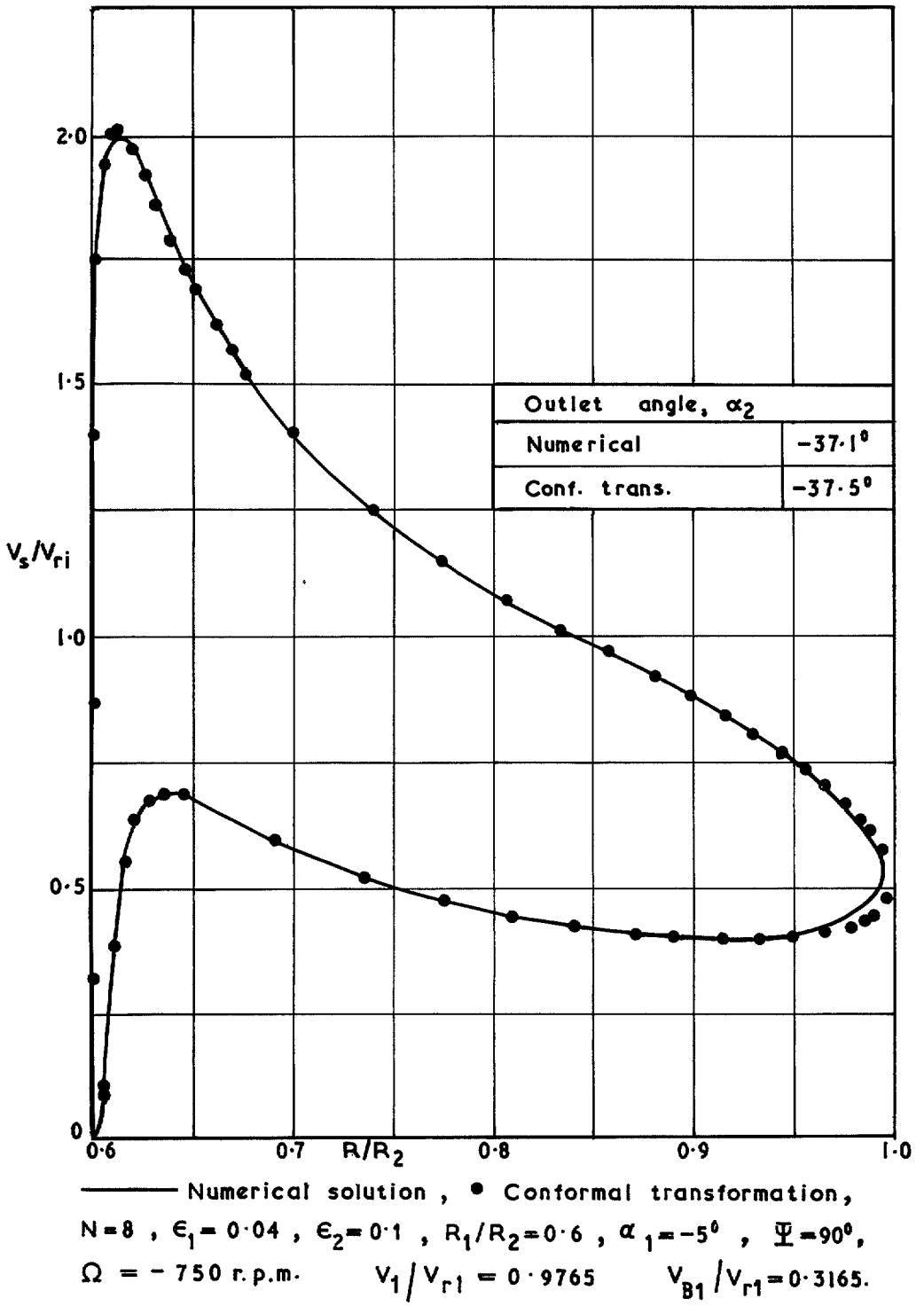

FIG. 12. Comparison of surface velocity distributions.

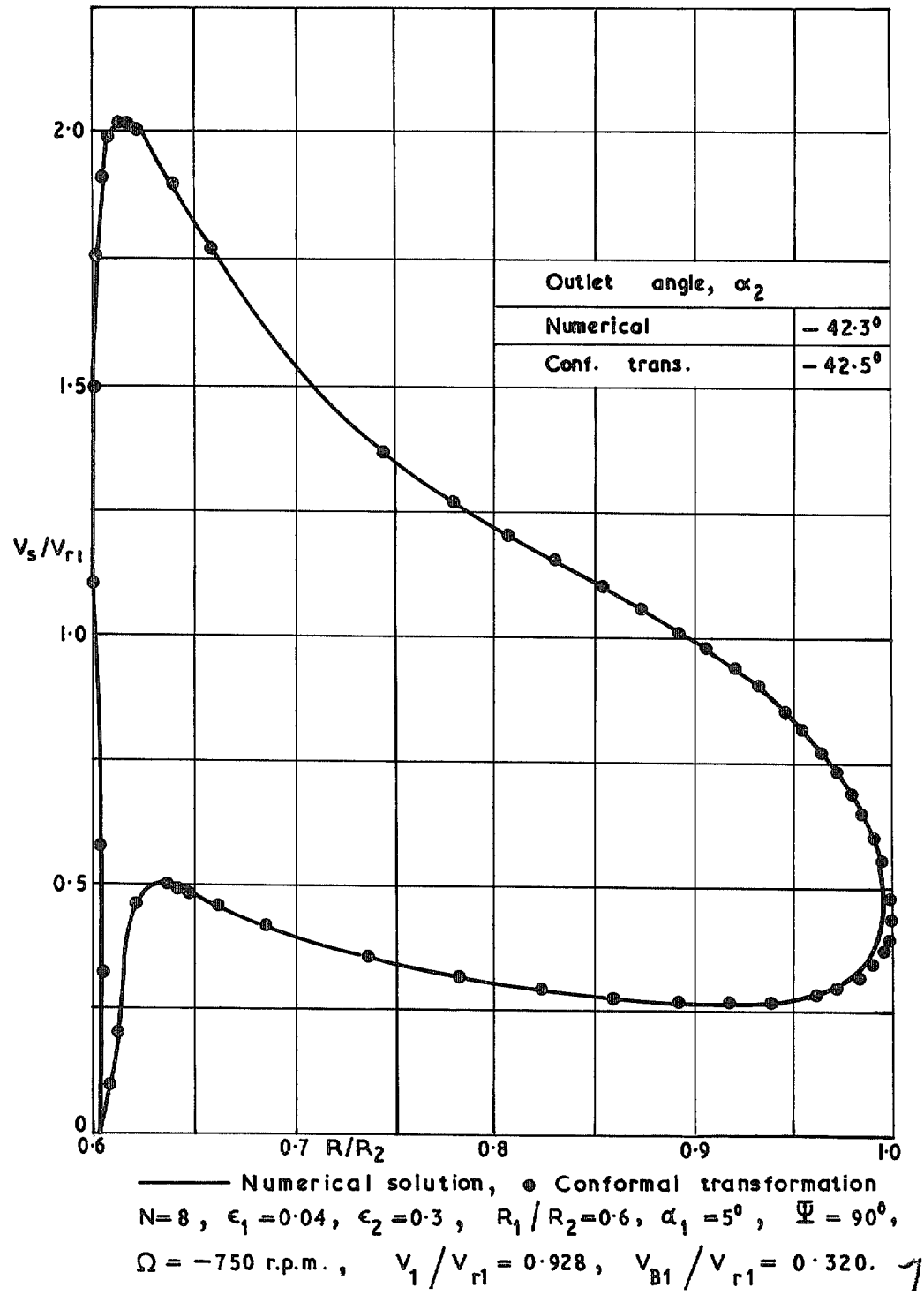

FIG. 13. Comparison of surface velocity distributions.

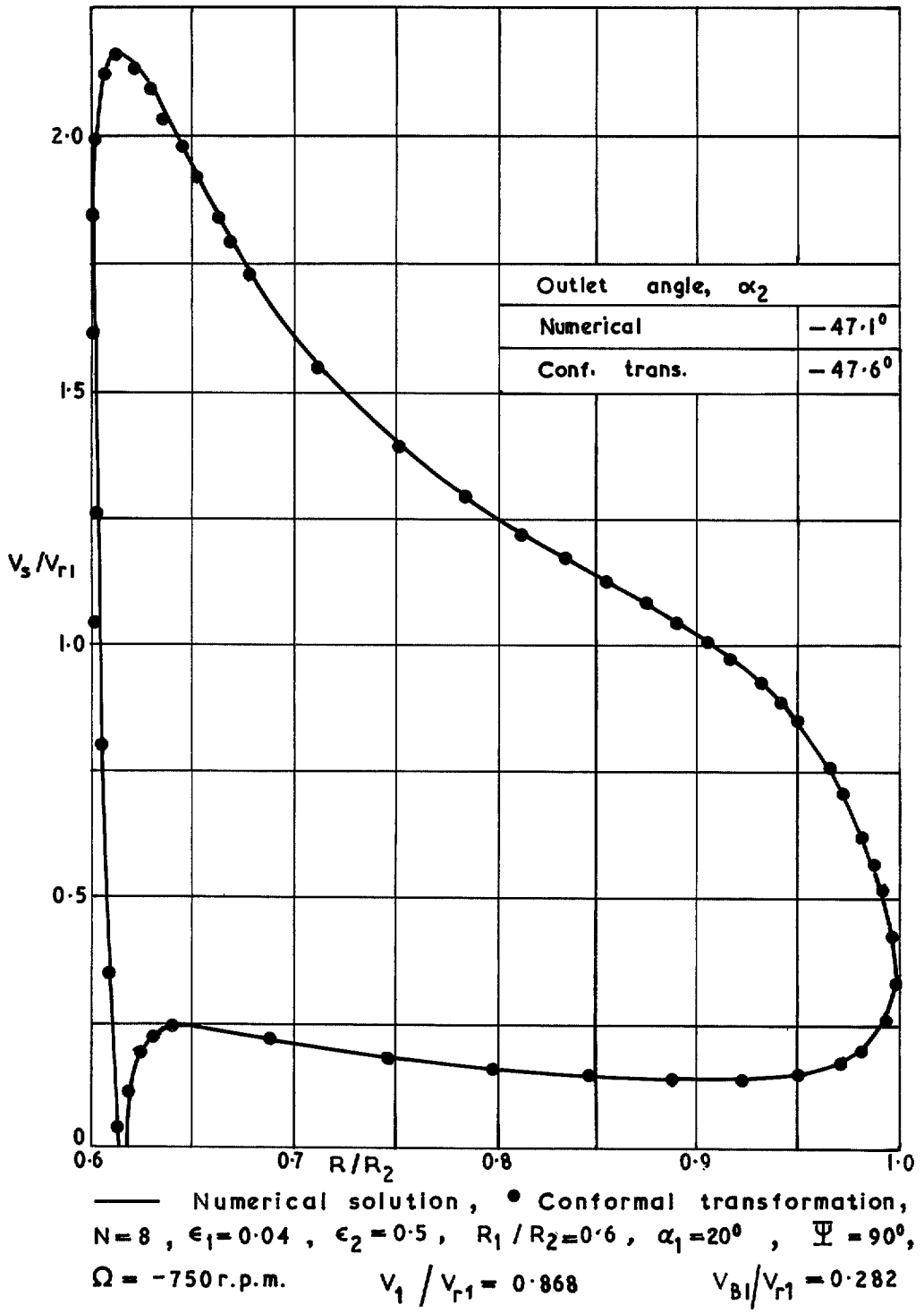

FIG. 14. Comparison of surface velocity distributions.

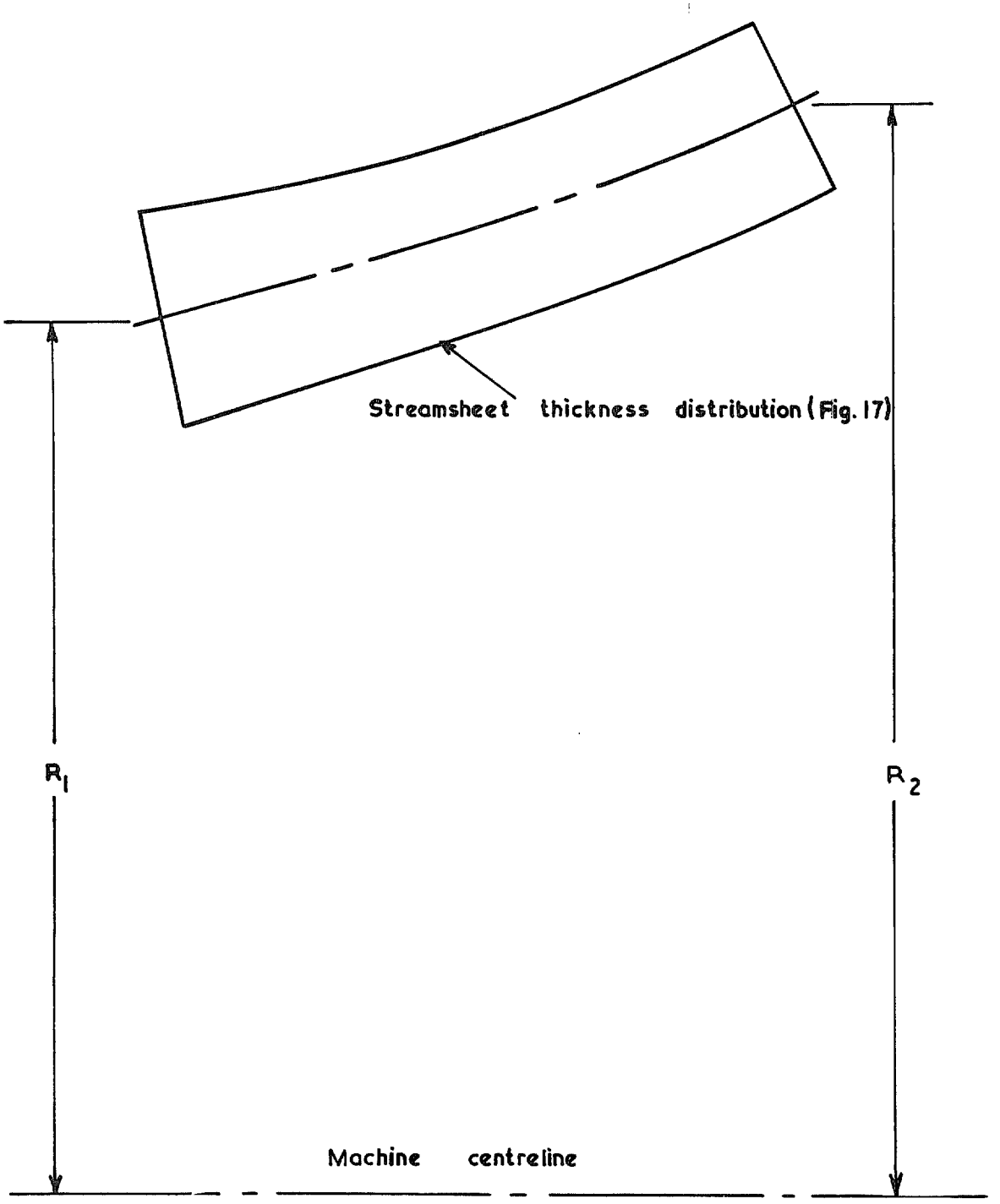

FIG. 15. Arbitrary streamsurface (used in Figs. 16 and 17).

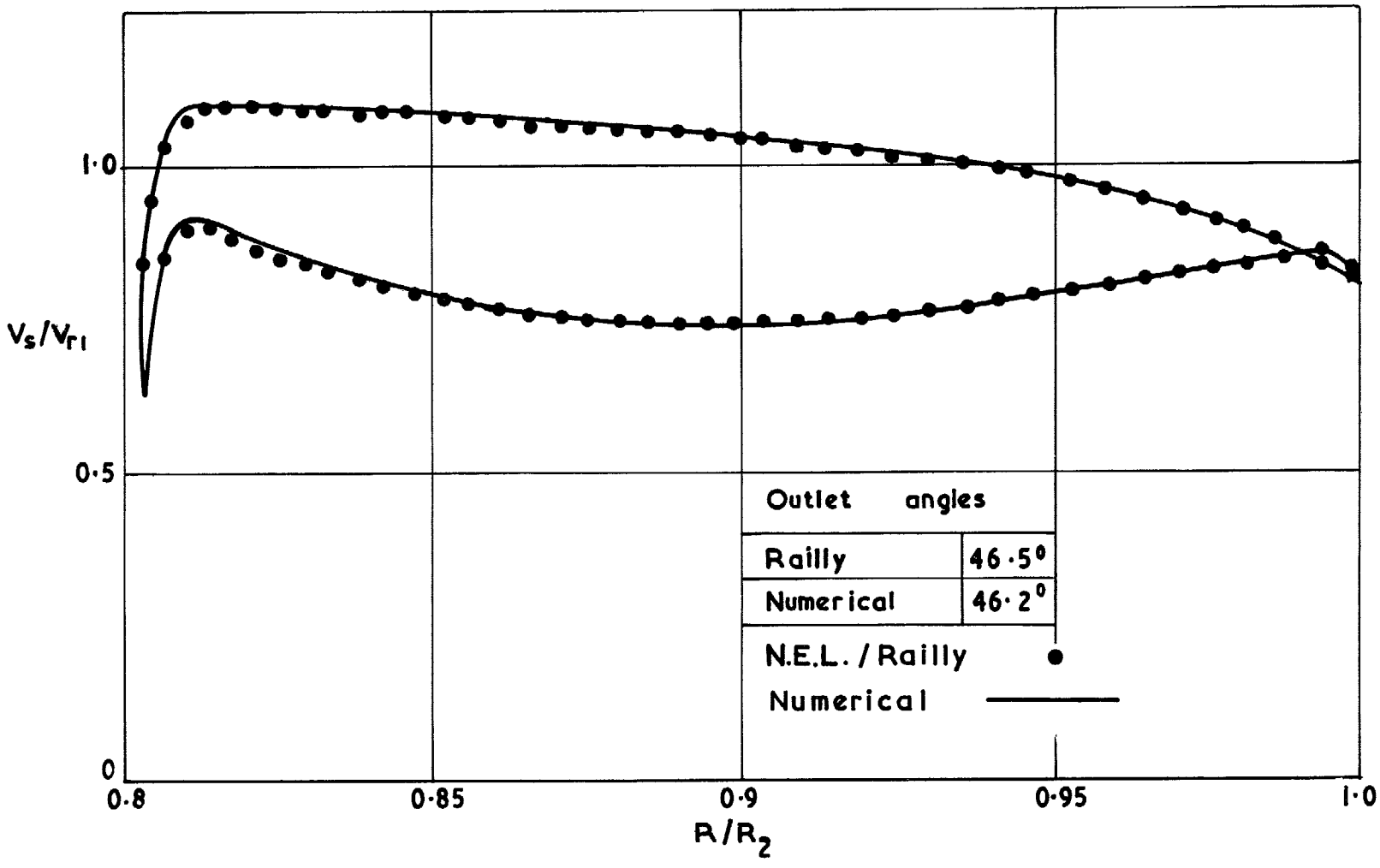

FIG. 16. Velocity distribution for arbitrary mixed-flow rotor of constant streamsheet thickness.

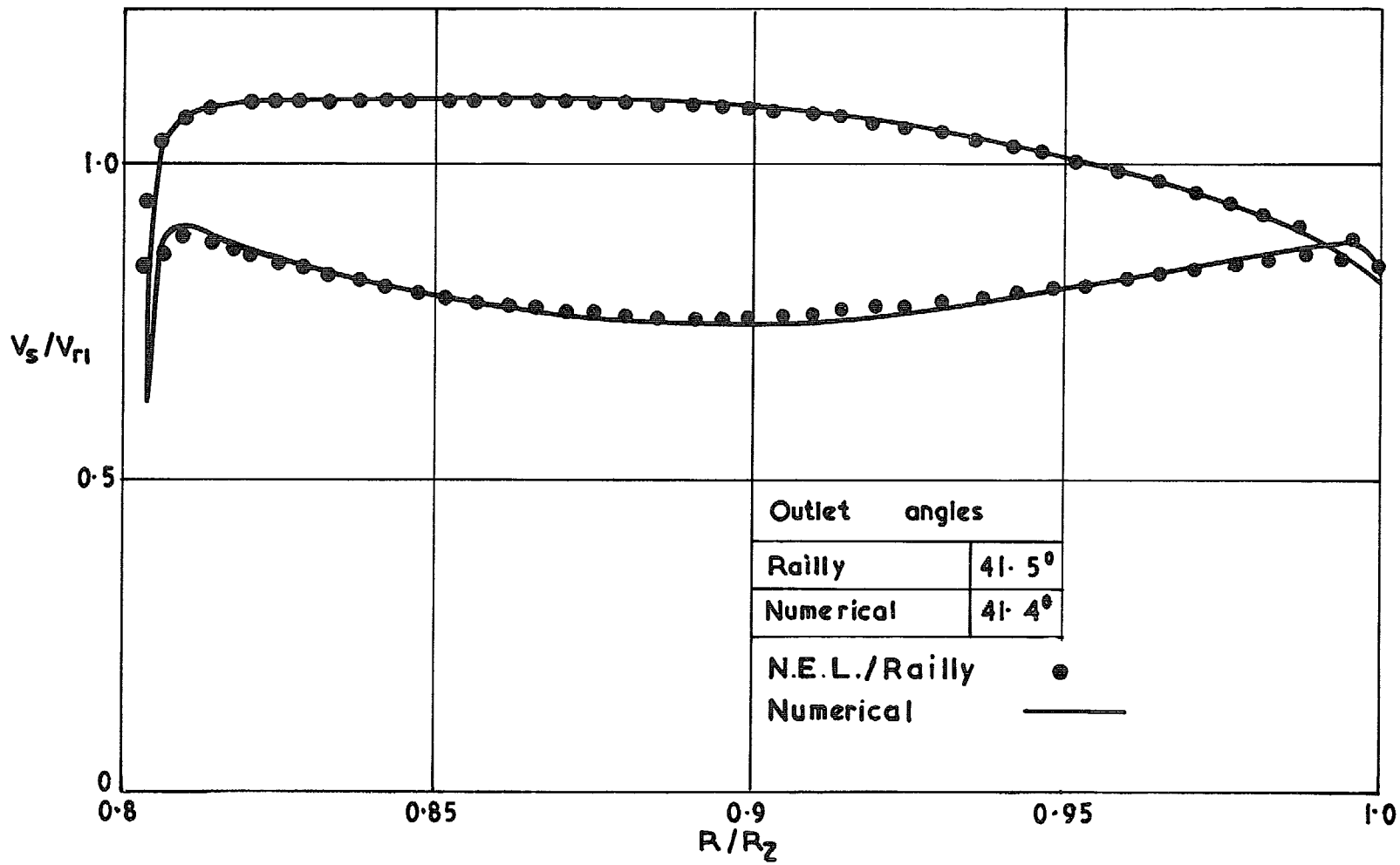

FIG. 17. Velocity distribution for arbitrary mixed-flow rotor of variable streamsheet thickness.

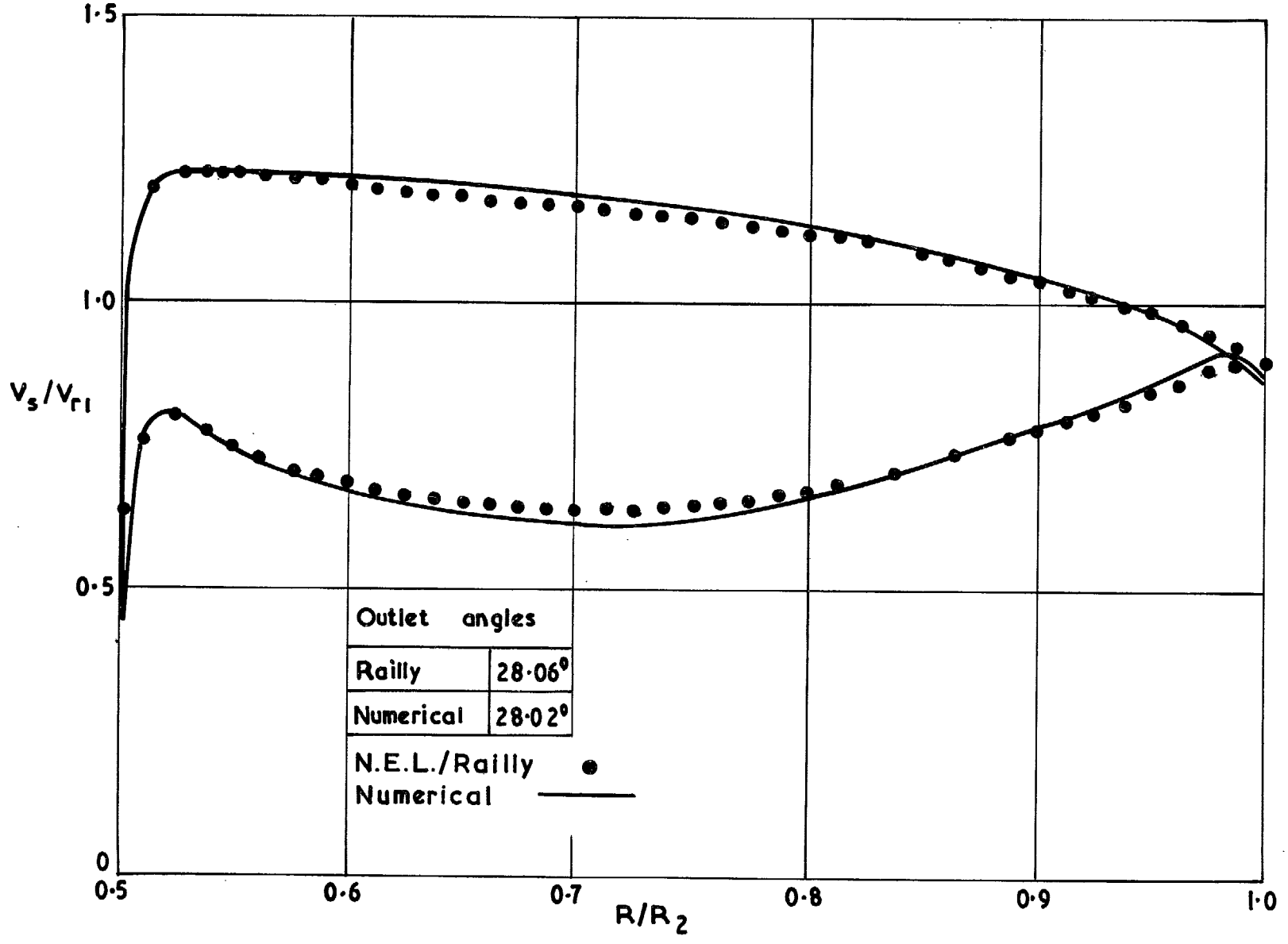

FIG. 18. Velocity distribution for variable thickness centrifugal rotor.

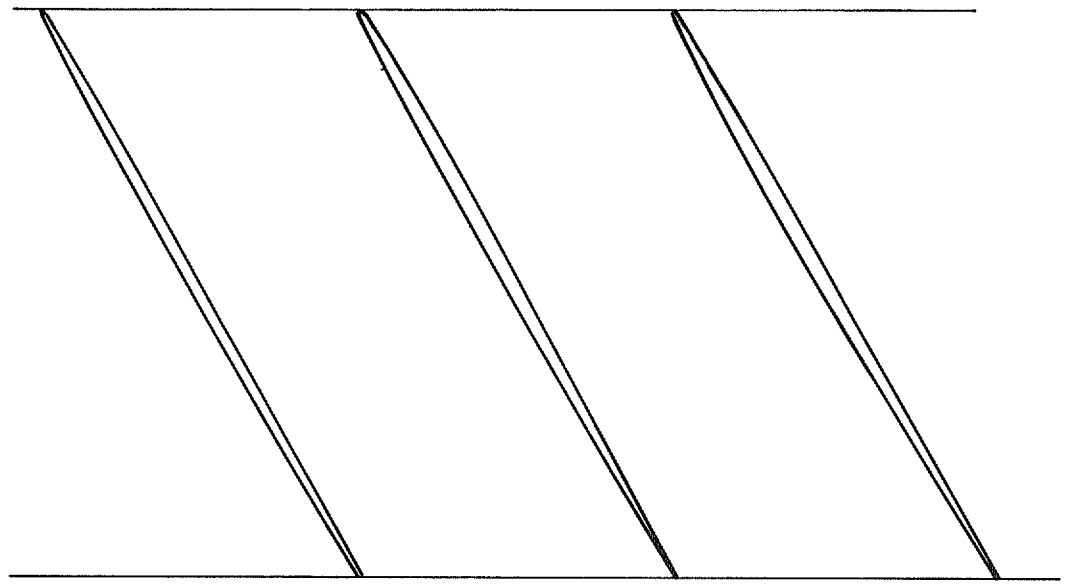

NACA 0001

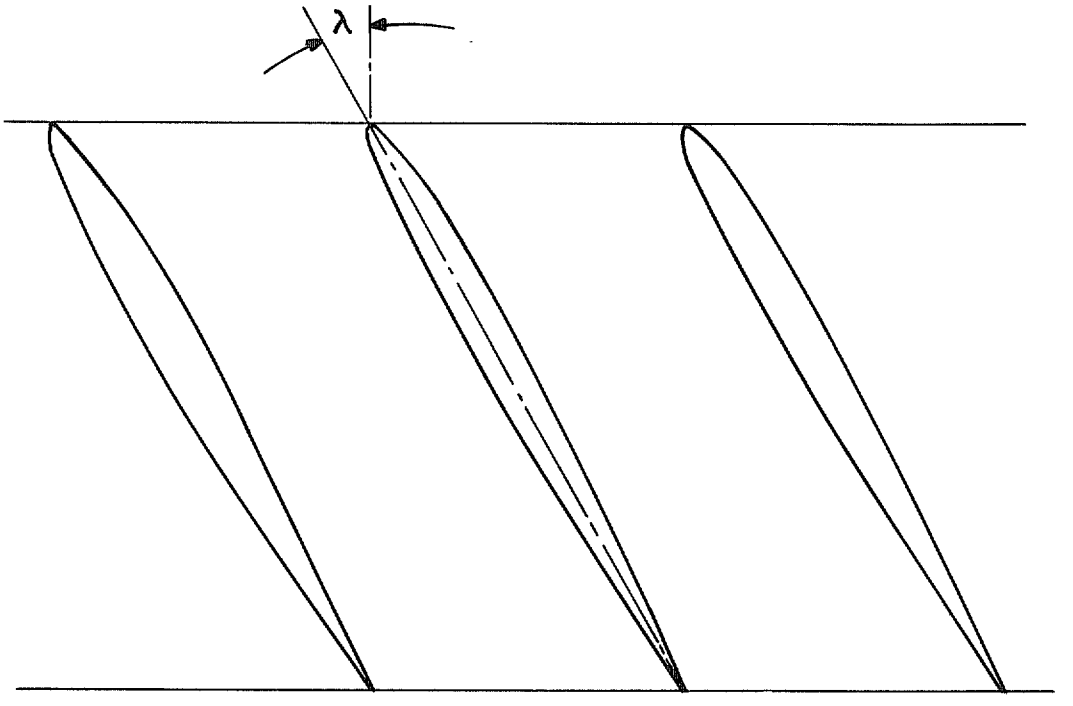

NACA 0006

FIG. 19. NACA four-digit profiles.

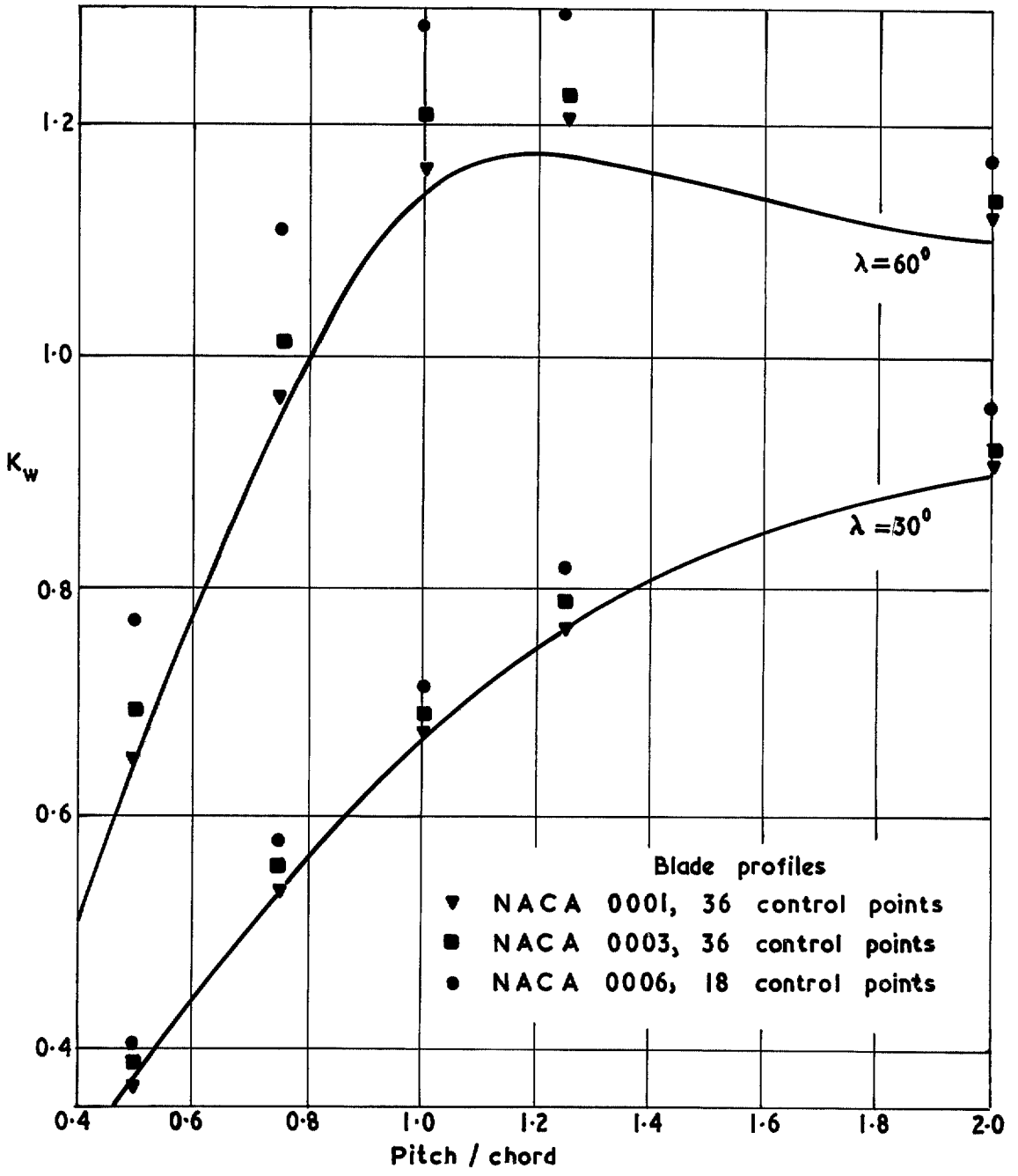

FIG. 20. Weinig coefficients, $K_W = C_L/C_{L_0}$, for flat plate cascades compared with numerical surface vorticity theory results for thin profiled blades.

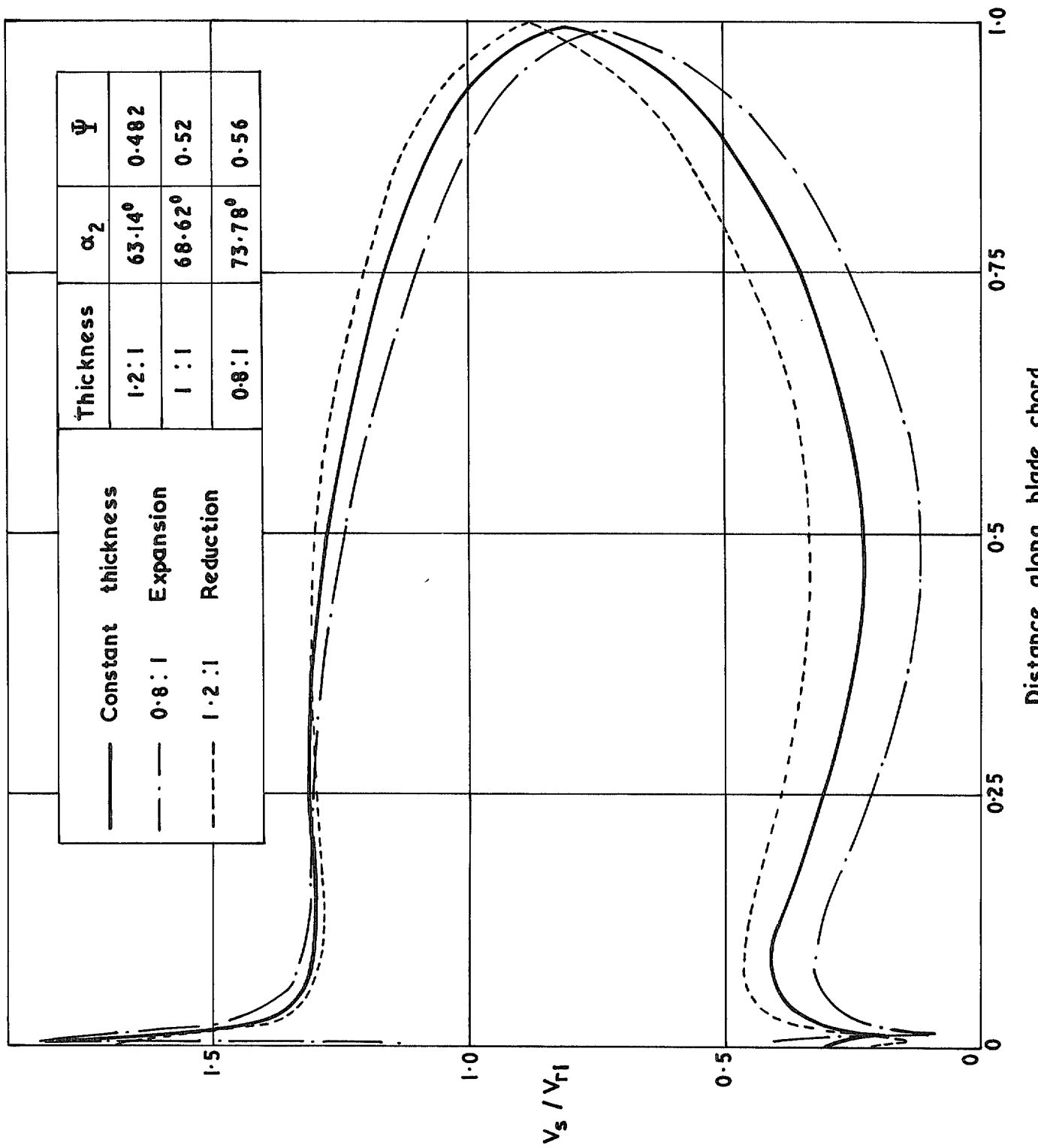

Printed in Wales for Her Majesty's Stationery Office by Allens Printers (Wales) Limited
Dd. 503426 K.5.

HER MAJESTY'S STATIONERY OFFICE
Government Bookshops
49 High Holborn, London WC1V 6HB
13a Castle Street, Edinburgh EH2 3AR
109 St Mary Street, Cardiff CF1 1JW
Brazennose Street, Manchester M60 8AS
50 Fairfax Street, Bristol BS1 3DE
258 Broad Street, Birmingham B1 2HE
80 Chichester Street, Belfast BT1 4JY
Government publications are also available through booksellers

R. & M. No. 3703

SBN 11 470503 8